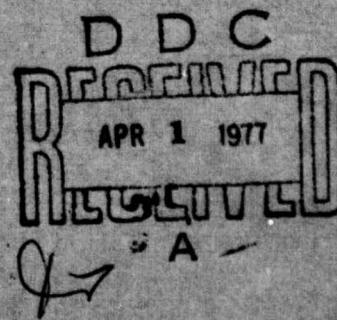
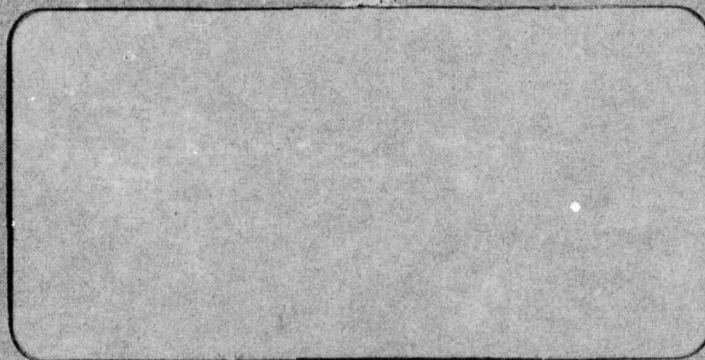
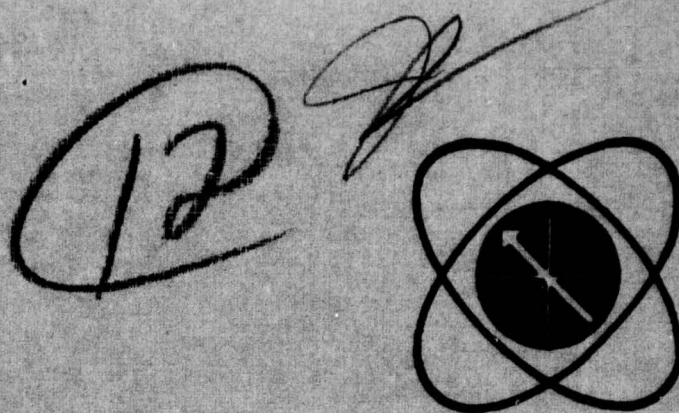


DDC FILE COPY

ADA037732



**DISTRIBUTION STATEMENT A**  
Approved for public release  
Distribution Unlimited

**MATHEMATICAL SCIENCES NORTHWEST, INC.**  
**P.O. BOX 1887      BELLEVUE, WASHINGTON 98009**

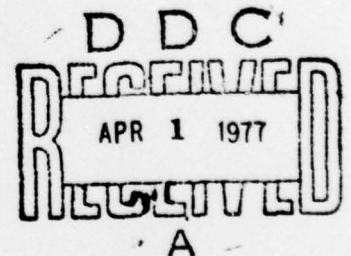
ELECTRICALLY INITIATED HCl CHEMICAL LASER  
AND  
THRESHOLD EXCITATION OF XeF AND KrF LASERS

Final Report  
Covering Work Performed During the Period  
July 15, 1974, to September 30, 1976

By

L.Y. Nelson, A.L. Pindroh, C.H. Fisher,  
S.R. Byron, and R.E. Center

MATHEMATICAL SCIENCES NORTHWEST, INC.  
P. O. Box 1887  
Bellevue, Washington 98009



February 1977

Contract N00014-75-C-0052

Sponsored by

Advanced Research Projects Agency  
ARPA Order No. 1807

Monitored by

Office of Naval Research  
Code 421

DISTRIBUTION STATEMENT A  
Approved for public release  
Distribution Unlimited

ARPA ORDER NO.: 1807  
PROGRAM CODE: 2E90  
NAME OF CONTRACTOR: Mathematical Sciences Northwest, Inc.  
EFFECTIVE DATE OF CONTRACT: July 15, 1974  
EXPIRATION DATE: September 30, 1976  
CONTRACT AMOUNT: \$338,965  
CONTRACT NUMBER: N00014-75-C-0052  
PRINCIPAL INVESTIGATOR: S. R. Byron  
(206) 827-0460  
SCIENTIFIC OFFICER: Director, Physics Programs  
Physical Sciences Division  
Office of Naval Research  
Department of the Navy  
800 North Quincy Street  
Arlington, Virginia 22217  
SHORT TITLE OF WORK: Electrically Excited HCl, XeF, and KrF Lasers  
DISCLAIMER: The views and conclusions contained in this document are those of the authors and should not be interpreted as necessarily representing the official policies, either expressed or implied, of the Advanced Research Projects Agency or the U. S. Government

ACCESSION for	
NTIS	White Section <input checked="" type="checkbox"/>
ORC	Buff Section <input type="checkbox"/>
UNANNOUNCED	<input type="checkbox"/>
JUSTIFICATION	
<i>Letter on file</i>	
BY	
DISTRIBUTION/AVAILABILITY CODES	
Dist.	AVAIL. and/or SPECIAL
<i>A</i>	



UNCLASSIFIED

SECURITY CLASSIFICATION OF THIS PAGE (When Data Entered)

REPORT DOCUMENTATION PAGE		READ INSTRUCTIONS BEFORE COMPLETING FORM
1. REPORT NUMBER 77-1049-1	2. GOVT ACCESSION NO.	3. RECIPIENT'S CATALOG NUMBER 9 30
4. TITLE (and Subtitle) Electrically Initiated HCl Chemical Laser and Threshold Excitation of XeF and KrF Lasers.	5. TYPE OF REPORT FINAL REPORT 15 July 1974 - Sept 30, 1976	6. PERFORMING ORG. REPORT NUMBER MSNW-77-1049-1
7. AUTHOR(s) L.Y./Nelson, A.L./Pindroh, C.H./Fisher, S.R./Byron R.E./Center	8. CONTRACT OR GRANT NUMBER(s) N00014-75-C-0052, ARPA Order-1807	9. PROGRAM ELEMENT, PROJECT, TASK AREA & WORK UNIT NUMBERS
10. PERFORMING ORGANIZATION NAME AND ADDRESS Mathematical Sciences Northwest, Inc. ✓ P. O. Box 1887 Bellevue, Washington	11. CONTROLLING OFFICE NAME AND ADDRESS 1265p.	12. REPORT DATE February 1977 ✓
13. MONITORING AGENCY NAME & ADDRESS (if different from Controlling Office) Office of Naval Research 800 North Quincy Street Arlington, VA 22217	14. SECURITY CLASS. (of this report) Unclassified	15a. DECLASSIFICATION/DOWNGRADING SCHEDULE
16. DISTRIBUTION STATEMENT (of this Report) <div style="border: 1px solid black; padding: 5px; text-align: center;">DISTRIBUTION STATEMENT A Approved for public release; Distribution Unlimited</div>		
17. DISTRIBUTION STATEMENT (of the abstract entered in Block 20, if different from Report)		
18. SUPPLEMENTARY NOTES		
19. KEY WORDS (Continue on reverse side if necessary and identify by block number) Electrically Initiated HCl Laser      Threshold Pump Power Densities HCl Chemical Laser Vibrationally Enhanced Reactions KrF and XeF Lasers		
20. ABSTRACT (Continue on reverse side if necessary and identify by block number) The report describes the results of two separate experimental investigations. The first concerns the electrical excitation of the HCl chemical laser and was motivated by the potential improvement of the laser performance by the vibrational enhancement of the reaction $\text{Cl} + \text{H}_2(v=1) \rightarrow \text{HCl}(v=v,1) + \text{H}$ . Detailed kinetic modelling of the e-beam and e-beam sustained discharge experiments was used in the interpretation of the experimental data. The rate constant for the vibrationally enhanced reaction was 40 times larger than for the reaction with $\text{H}_2(v=0)$ at $T = 300^\circ\text{K}$ . This enhanced rate is not fast enough to lead to $\rightarrow \text{OVER}$		



20. Abstract (continued)

efficient use of the  $H_2(v=1)$  excited by electron impact. The maximum electrical to laser conversion efficiency obtained was 3 percent.

The second part of the report describes measurements of the threshold pumping power density in e-beam sustained discharge excitation of KrF and XeF lasers. Stable discharges were obtained in Ar-Kr-F<sub>2</sub> and Ar-Xe-NF<sub>3</sub> mixtures at 1 atm for times greater than 0.5  $\mu$ sec and lasing pulse width as long as 0.5  $\mu$ sec. The threshold pump power densities varied inversely with the cavity build up time. Based on the present results it is evident that efficient laser operation in KrF and XeF could be achieved in a 1-m long sustained discharge with input power densities in the range of 50 to 100 kW/cm<sup>2</sup> over a 1  $\mu$ sec time scale.

Cu

MICROSECOND

## PREFACE

This report is presented in two parts. The first concerns the investigation of e-beam controlled discharge initiation of the HCl chemical laser system. The second part describes an experimental investigation of the threshold power density requirements for e-beam sustained discharge excitation of XeF and KrF.

This research was supported by the Advanced Research Projects Agency of the Department of Defense and was monitored by ONR under Contract No. N00014-75-C-0052.

PART A

ELECTRICALLY INITIATED HCl CHEMICAL LASER



## PART A

### CONTENTS

SECTION		PAGE
I	INTRODUCTION	1
II	DESCRIPTION OF EXPERIMENT	4
III	EXPERIMENTAL RESULTS	11
	A. Laser Pulse Shape and Spectroscopic Analysis	11
	B. Chlorine Visible Absorption Measurements	18
	C. Laser Energy Measurements	18
IV	COMPUTER MODEL DESCRIPTION AND COMPARISONS WITH EXPERIMENT	24
	A. Analytical Model of Electron Beam and Electric Discharge Physics	24
	e-Beam Physics	24
	Discharge Physics	26
	B. Chemical Kinetics and Laser Gain Computer Model	29
	C. Computer Model Comparisons with Experimental Observations	36
V	CONCLUSIONS	51
	REFERENCES	53

## PART A

### FIGURES

FIGURE		PAGE
1.	Schematic Diagram of the HCl Laser Excitation Apparatus	5
2.	Cross-Sectional View of Cold Cathode Electron Gun and Discharge Chamber	6
3.	Schematic Diagram of the Optical Arrangement for the Chlorine Absorption Measurements	8
4.	Experimentally Measured HCl Laser Pulse Shapes for Electron Beam and Discharge Excitation (1- $\mu$ sec Pulse Duration)	12
5.	Time Histories and Relative Intensities of the HCl Laser Transitions Observed Using Only the Electron Beam for Excitation	14
6.	Time Histories and Relative Intensities of the HCl Laser Transitions Observed in Low E/N ( $1.55 \times 10^{-16}$ V-cm <sup>2</sup> ) Discharge Excitation	15
7.	Time Histories and Relative Intensities of the HCl Laser Transitions Observed in High E/N ( $2.5 \times 10^{-16}$ V-cm <sup>2</sup> ) Discharge Excitation	16
8.	Reconstructed HCl Laser Pulse Shape Using the Low E/N Discharge Data Presented in Figure 6	17
9.	Rate of Chlorine Disappearance in the High E/N ( $2.5 \times 10^{-16}$ V-cm <sup>2</sup> ) Discharge	19
10.	Measured HCl Laser Energy as a Function of Cl <sub>2</sub> and H <sub>2</sub> Mole Fractions Using Electron Beam Excitation	20
11.	Measured HCl Laser Energy as a Function of Cl <sub>2</sub> Mole Fraction Using Discharge Excitation at Constant Energy Input	22
12.	Drift Velocity and Characteristic Electron Energy for an Ar/H <sub>2</sub> Mixture	27
13.	Boltzmann Calculations for an Ar/H <sub>2</sub> (50/50) Mixture	28

FIGURE		PAGE
14.	HCl-H <sub>2</sub> and HCl-Ar Optical Broadening Coefficients	34
15.	Rate of Chlorine Disappearance Using Only the Electron Beam for Excitation	37
16.	Calculated HCl Chemical Laser Pulse Shape for all Lines and the 2-1 H <sup>37</sup> Cl Line with Electron Beam Excitation	39
17.	Calculated HCl Laser Pulse Shape for Low E/N ( $1.55 \times 10^{-16}$ V-cm <sup>2</sup> ) Discharge Excitation	41
18.	Calculated HCl Laser Pulse Shape for Low E/N ( $1.55 \times 10^{-16}$ V-cm <sup>2</sup> ) Discharge Excitation	43
19.	Calculated HCl Chemical Laser Pulse Shape for Low E/N ( $1.55 \times 10^{-16}$ V-cm <sup>2</sup> ) Discharge Excitation (Current Density, 24 A/cm <sup>2</sup> )	44
20.	Calculated HCl Chemical Laser Pulse Shape for High E/N ( $2.5 \times 10^{-16}$ V-cm <sup>2</sup> ) Discharge Excitation (Current Density, 24 A/cm <sup>2</sup> )	45
21.	Comparison of Experimentally Determined Band Intensities with Calculated Profiles for the 1-0, 2-1, and 3-2 H <sup>35</sup> Cl Laser Transitions for the Low E/N ( $1.55 \times 10^{-16}$ V-cm <sup>2</sup> ) Discharge Case	46
22.	Rate of Chlorine Disappearance Measured in the Low E/N ( $1.55 \times 10^{-16}$ V-cm <sup>2</sup> ) Discharge	49



## PART A

### TABLES

TABLE		PAGE
1.	Selected Reaction Rate Constants for HCl Chemical Laser ( $T = 300\text{ }^{\circ}\text{K}$ )	2
2.	Summary of Laser Output Energies and Electrical Efficiencies	23
3.	Rate Coefficients for the HCl Chemical Laser System	30

## SECTION I

### INTRODUCTION

The rate of an endothermic chemical reaction can be significantly increased by vibrational excitation of the reactant molecules.<sup>1,2</sup> For the near thermoneutral reaction  $\text{Cl} + \text{H}_2 \rightarrow \text{HCl}$  ( $\Delta H \approx 1 \text{ kcal}$ ), theoretical and experimental estimates have been made for the accelerated reaction rate of vibrationally excited  $\text{H}_2$ . Estimates range from a factor of  $25^{3,4}$  to  $2000^5$  for the ratio of rate constants  $k_{\text{H}_2}(v=1)/k_{\text{H}_2}(v=0)$ . If the larger factor were correct, substantial improvements could be expected in the performance of the electrically excited HCl chemical laser. The reason for this improvement can be understood by considering the rate data presented in Table 1. Reactions (1) and (2) constitute the HCl chain reaction steps leading to an HCl laser. Reaction (2) is the slower rate-controlling step which must regenerate H atoms for the highly exothermic "hot" reaction (1). Laser operation, therefore, dictates a high initial H or Cl atom density which could produce rapid V-T deactivation of excited HCl molecules and reduced laser efficiency. If, on the other hand, reaction (3) were three orders of magnitude faster than (2), 100 times smaller concentrations of Cl atom would be required at modest hydrogen vibrational temperatures (2000 °K) to produce the same total rate of H-atom production as reaction (2).

The goal of the present study was to investigate the performance of an HCl chemical laser making use of reaction (3) and to evaluate the magnitude of the rate enhancement. A short pulse (1  $\mu\text{sec}$ ) electron beam stabilized discharge has been used to initiate the HCl chemical laser in mixtures of Ar,  $\text{H}_2$ , and  $\text{Cl}_2$ . Reliable estimates could be made for the degree of  $\text{H}_2$  vibrational excitation since the electron energy distribution is fairly well characterized for these externally ionized discharges. A comprehensive computer model of the HCl laser and chemical kinetics used the estimates

Table 1

Selected Reaction Rate Constants for HCl Chemical Laser ( $T = 300\text{ }^{\circ}\text{K}$ )

Reaction	Rate Constant ( $\text{cm}^3/\text{mole}\cdot\text{sec}$ )
1. $\text{H} + \text{Cl}_2 \xrightarrow{k_{\text{hot}}} \text{HCl} (v=1,2,3,\dots) + \text{Cl}$	$3.8 \times 10^{12}$
2. $\text{Cl} + \text{H}_2 \xrightarrow{k_{\text{cold}}} \text{HCl} (v=0) + \text{H}$	$1.5 \times 10^{10}$
3. $\text{Cl} + \text{H}_2 (v=1) \rightarrow \text{HCl} (v'=0,1) + \text{H}$	$6.3 \times 10^{11}$
4. $\text{Cl} + \text{HCl} (v=1) \rightarrow \text{HCl} (v+0) + \text{Cl}$	$4.8 \times 10^{12}$
5. $\text{H} + \text{HCl} (v=1) \rightarrow \text{HCl} (v=0) + \text{H}$	$4.0 \times 10^{12}$



for hydrogen vibrational excitation to calculate the energies and intensities of the various HCl vibrational laser transitions and time-dependent concentrations of the excited HCl levels ( $v=0,1,2,3$ ), H and Cl atoms, Cl<sub>2</sub> and H<sub>2</sub> ( $v=0,1$ ).

Three principal diagnostic tools were used to study the HCl chemical laser under a variety of discharge conditions. Time-resolved spectroscopic measurements were made of the overall pulse shape and the individual HCl laser lines, for both H<sup>35</sup>Cl and H<sup>37</sup>Cl isotopes. Consumption of the Cl<sub>2</sub> was monitored using visible absorption spectroscopy. Laser output energy measurements were also made as an additional constraint for evaluating the vibrationally enhanced reaction rate constant with the computer model.

Good agreement between the experimental measurements and the computer simulation has been achieved and will be described more fully in the main text. A value of 40 for the vibrational rate enhancement ( $k_{H_2}(v=1)/k_{H_2}(v=0)$ ) has been found to be consistent with the experimental observations.

Sections II and III describe the experimental apparatus, the operating characteristics of the HCl chemical laser, and the diagnostic measurements. A computer model of the reaction kinetics and laser characteristics are presented in Section IV together with comparisons with experimental measurements.

## SECTION II

### DESCRIPTION OF EXPERIMENT

Figure 1 is a general schematic diagram of the laser excitation apparatus and diagnostics. The laser cavity was formed by two 2-m radii-of-curvature totally reflective mirrors (R).  $\text{CaF}_2$  flats were used as laser windows (W) and output coupler (O). Infrared detector (I) and monochromator (M) measured the time-resolved spectroscopic content of the laser pulse. An energy meter (E) and infrared detector (I') were used at other times to measure the total laser energy and pulse shape. A short-pulse (1  $\mu\text{sec}$ ) cold-cathode electron beam source was used to stabilize discharges in mixtures of Ar,  $\text{H}_2$ , and  $\text{Cl}_2$ . A cross-sectional drawing of the essential features of the discharge chamber and electron-beam emitter structure is shown in Figure 2. The electron gun operated at 160 kV and delivered 3.5 A/cm<sup>2</sup> through the 1-mil aluminized Kapton foil which separated the discharge chamber from the diode vacuum chamber. By adjusting the spacing from the graphite (or thin tantalum foil) emitter to the electron-beam anode screen, the current pulse amplitude and duration could be altered. Experiments were successfully run with 10- $\mu\text{sec}$  pulse durations at 0.3 to 0.4 A/cm<sup>2</sup> current densities.

The discharge chamber consisted of a high-density polyethylene body which provided high-voltage electrical isolation for the aluminum anode as shown in Figure 2. An array of 10 coaxial cables connected the discharge anode to a triggered gas switch and 2- $\mu\text{F}$  energy storage capacitor. Electronic delay circuits allowed the discharge to be fired at any time with respect to a trigger pulse which initiated the electron gun. The discharge current rise time was typically 200 to 300 nsec and was limited by the inductance of the connecting cables and capacitor (approximately 100 nH). The optical aperture of the discharge region is reduced by a 2-cm diameter channel in the high density polyethylene at each Brewster angle window as shown in Figure 1. Figure 2 schematically shows the effective system optical

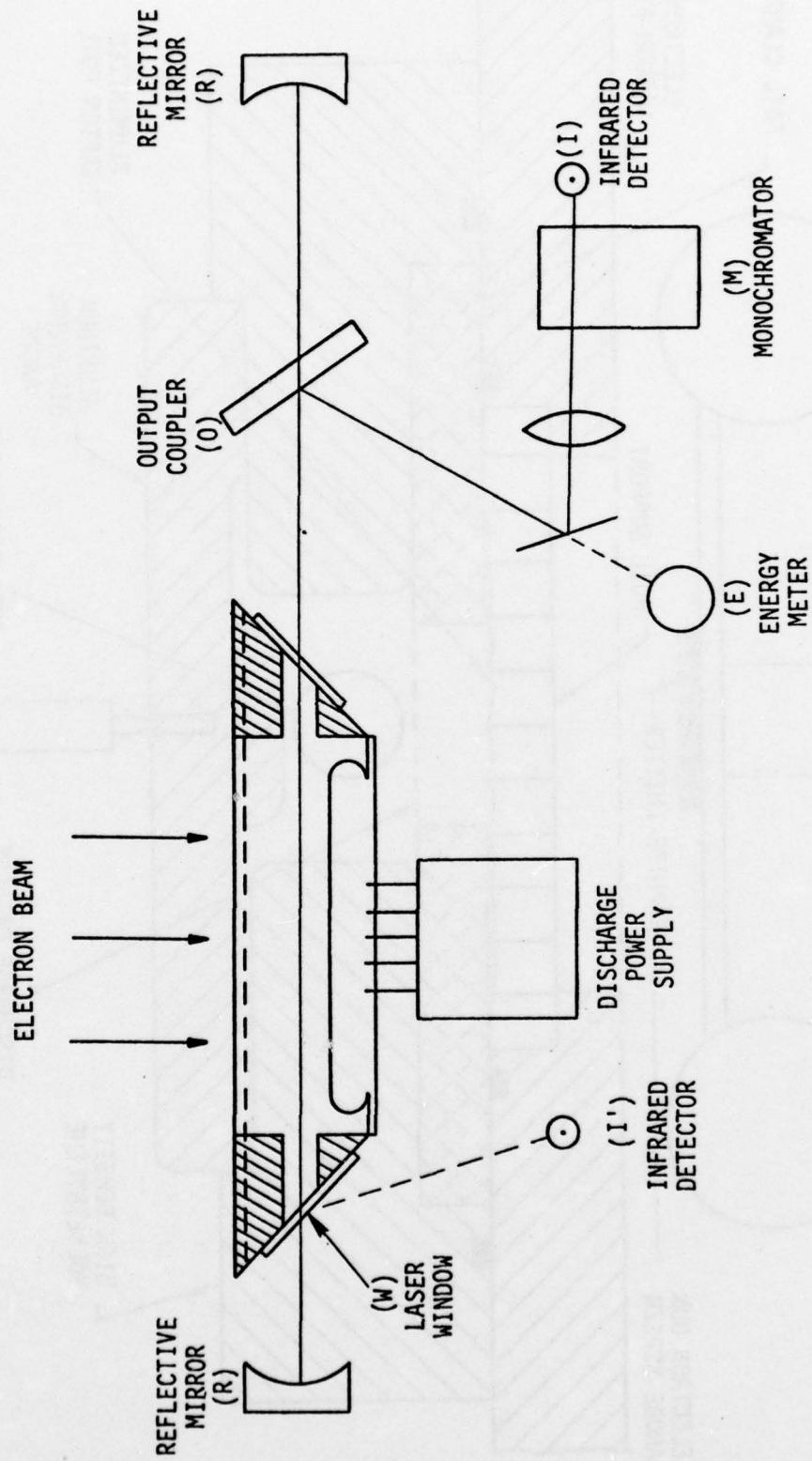


Figure 1. Schematic Diagram of the HCl Laser Excitation Apparatus



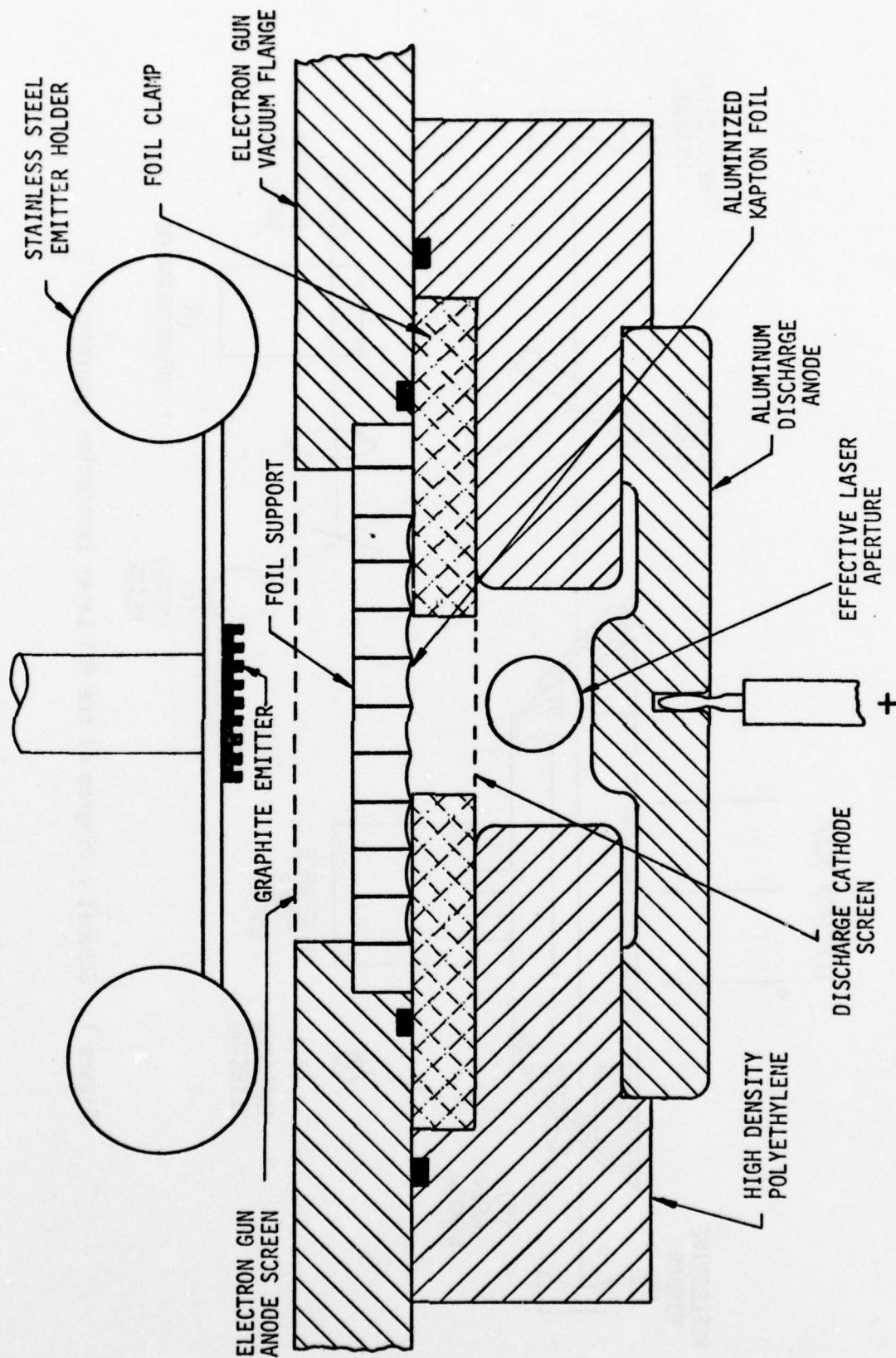


Figure 2. Cross-Sectional View of Cold Cathode Electron Gun and Discharge Chamber. For illustration purposes, the electron beam foil support structure is shown with vanes running parallel to the laser axis, whereas the vanes actually were transverse to the axis.

aperture with respect to the 5-cm wide discharge anode. The discharge anode was 50 cm long, and the overall length of the chamber was 75 cm. Chlorine absorption measurements, to be described later, indicated very little  $\text{Cl}_2$  disappearance for 5-or 10-minute sample storage times in the cavity. The white polyethylene walls adjacent to the discharge region did discolor after several hundred shots, partly due to radiation damage from the electron beam.

The argon, hydrogen, and chlorine gases were obtained from Matheson and were either pre-purified grade ( $\text{Ar}$ ,  $\text{H}_2$ ) or high purity grade ( $\text{Cl}_2$ ), and were used without further purification. The stated purities were 99.998% for  $\text{Ar}$ , 99.95% for  $\text{H}_2$ , and 99.5% for  $\text{Cl}_2$ . Matheson flowmeters were used to adjust the relative concentrations of the gases. The meters were connected together and the gases flowed through 13 ft of copper tubing (1/4-in. OD, 1/8-in. ID) for good mixing before entering the discharge chamber. There was a 20 to 30 percent difference in the laser output energies observed under static and flowing gas conditions. The overall laser spectrum and pulse shape were essentially the same for both conditions. All the chlorine visible absorption data were taken using flowing gas mixtures.

Spectroscopic measurements of the individual  $\text{HCl}$  laser transitions were made with quarter-meter (Jarrel-Ash) and one-meter (McPherson) grating monochromators. The frequency resolution of the smaller instrument was  $\pm 0.8 \text{ cm}^{-1}$ . Higher resolution,  $\pm 0.2 \text{ cm}^{-1}$ , was obtained using the one-meter monochromator, thereby permitting unambiguous identification of the  $\text{H}^{37}\text{Cl}$  lines. Individual  $\text{H}^{35}\text{Cl}$  and  $\text{H}^{37}\text{Cl}$  P-branch transitions were recorded in a shot-by-shot search of their respective vibrational bands. A cooled (77 °K) gold-doped germanium detector (Raytheon, QKN 1568), 100-nsec rise time, was used for all the infrared laser measurements. Matching 100  $\Omega$  coaxial cable and resistive terminator were used for optimum time response.

Figure 3 shows the experimental optical arrangement used for the chlorine absorption measurements. A high brightness, 100-watt mercury arc

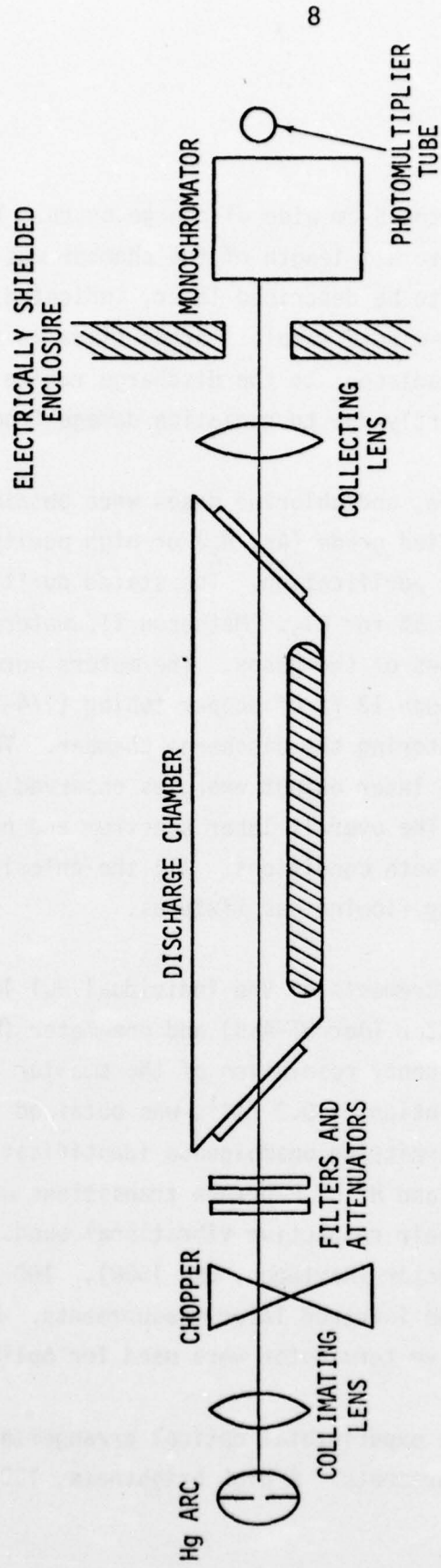


Figure 3. Schematic Diagram of the Optical Arrangement for the Chlorine Absorption Measurements



lamp (Osram, HBO 100 W/2) provided an intense 365 nm source. Four Corning glass filters (two each 5860 and 5840) were used to isolate the 365-nm spectral region emitted by the source. Care was taken to further attenuate the light emitted by the mercury arc using screens so that significant chlorine dissociation did not occur. Two criteria were established for determining the maximum light flux which could be transmitted through the gas samples. First, the measured absorption did not decrease over a 10- or 15-minute time span with the gas sample slowly flowing through the discharge chamber. As a second check for pre-reaction, the chlorine mole fraction measured by the visible absorption technique should agree within 10 percent with the concentration found using the relative filling time of the discharge chamber (typically over the range 100 to 300 torr) with each of the three component gases. Since the mercury arc operated DC and the experimental measurements were pulsed, a chopper wheel with a single 1 in. opening, operating at 1725 rpm, provided additional attenuation by reducing the duty cycle of the arc illumination of the sample. A photodiode viewing the light reflected from the glass filters provided a synchronization signal for the electron beam and discharge circuitry. A zero percent baseline absorption was measured for each experiment by shutting off the chlorine flow following an excitation pulse, waiting 3 to 4 minutes for the flowing argon and hydrogen to purge the chamber of chlorine, and then recording the light signal on the oscilloscope. One-hundred percent absorption was also recorded on the same oscilloscope trace by physically blocking the light reaching the detection system.

Two problems encountered in these measurements were the light emitted by the discharge itself and the electrical noise generated by the electron beam and discharge. The latter difficulty was remedied using a shielded and electrically-isolated Faraday cage for the photomultiplier and its associated electronics (power supply and oscilloscope). A quarter-meter monochromator was used with the photomultiplier to alleviate the background luminosity problem. Attenuation of the mercury arc source was also adjusted for maximum light flux to overcome background emission from the discharge chamber.



A Gen-Tec energy meter (ED-200) was used to measure the total single-pulse HCl laser energy. When the energy meter was used, an infrared detector monitored the laser pulse time history (Fig. 1). A tilted  $\text{CaF}_2$  flat inside the laser cavity provided approximately 8 percent output coupling (round-trip) at 30 degrees incidence angle. The total cavity losses were estimated to be 13 percent when mirror reflectivity losses and scattering from window surfaces were included.

### SECTION III

#### EXPERIMENTAL RESULTS

##### A. Laser Pulse Shape and Spectroscopic Analysis

HCl laser pulse time histories for three different excitation conditions are shown in Figure 4. The gas composition (Ar/H<sub>2</sub>/Cl<sub>2</sub> 49.1/49.1/1.8) and pressure (400 torr) were the same for all three examples presented. The electron beam and electric discharge initiation pulses began at  $t = 0$  and were terminated at  $t = 1 \mu\text{sec}$ . Using the electron beam alone for initiation of the chemical laser always produces a pulse with three prominent peaks as seen in Figure 4(a). Two different values of E/N were extensively studied. A low value ( $1.55 \times 10^{-16} \text{ V-cm}^2$ ) was found which significantly enhanced the laser output compared to the electron beam alone for initiation. The high E/N value ( $2.5 \times 10^{-16}$ ) was the maximum voltage the apparatus could reliably withstand without arc formation in the laser gas. The pulse shape of the low E/N discharge-initiated HCl laser was also quite characteristic and reproducible. High E/N discharges produced laser pulses which did vary somewhat from day-to-day, although the overall characteristics were a short duration (typically 2.1  $\mu\text{sec}$ ) and smooth, steep drop-off after the laser reached maximum intensity. On some traces, three small distinct peaks spaced by approximately 150 nsec, or two peaks, spaced by 300 nsec, were seen superimposed on the general peak intensity curve, for the high E/N laser pulses. Some of this variability in the appearance of the peak laser intensity was correlated with slight variations (100 to 200 nsec) in the electron beam pulse duration, which is essentially the same as the discharge pulse duration.

Longest duration lasing was observed for low E/N or low-energy input discharges at 400 torr. The slightly earlier laser threshold time of the high E/N case (Figure 4(c)) can be qualitatively explained by the higher H-atom and H<sub>2</sub>(V) production rates in the more energetic discharge. Molecular chlorine consumption by the chemical reaction and buildup of chlorine atoms causes the pulse to end quite abruptly. The enhanced cold reaction rate caused by hydrogen vibrational excitation is qualitatively evident in Figure 4(b) as the low-intensity, long duration tail of the laser pulse.

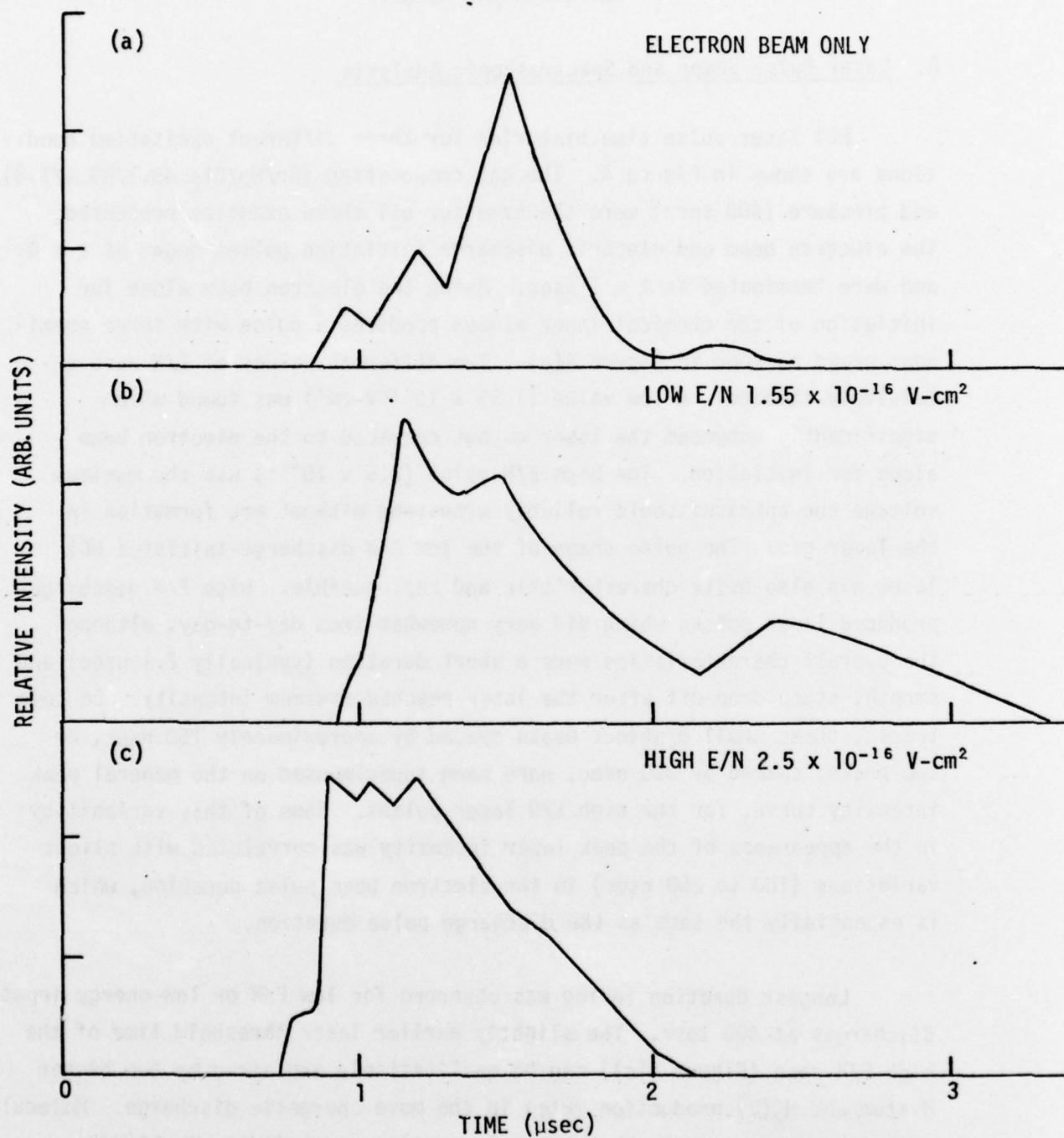


Figure 4. Experimentally Measured HCl Laser Pulse Shapes for Electron Beam and Discharge Excitation (1-μsec Pulse Duration). Gas pressure and mixture were 400 torr and Ar/H<sub>2</sub>/Cl<sub>2</sub> 49/49/2.

Detailed spectroscopic measurements were made for the three cases of Figure 4, and this information is graphically presented in Figures 5, 6, and 7. Laser emission from 3-2 transitions was generally much weaker than 2-1 and 1-0 bands. Only in the electron beam initiation case (Fig. 5) did the 1-0 transitions reach threshold significantly later than the 3-2 and 2-1 bands. The late-time emission in the low E/N discharge experiments was dominated by 1-0 transitions.

Individual  $\text{H}^{37}\text{Cl}$  laser lines were identified and time resolved using the one-meter monochromator. The average spacing of a pair of  $\text{H}^{35}\text{Cl}$  and  $\text{H}^{37}\text{Cl}$  lines is  $1.8\text{ cm}^{-1}$ , which is essentially the resolution limit of the smaller quarter-meter instrument. However, accidental near coincidences, such as 2-1 P(7)  $\text{H}^{37}\text{Cl}$  and 1-0 P(11)  $\text{H}^{35}\text{Cl}$  ( $\Delta\nu = 0.6\text{ cm}^{-1}$ ), were only resolvable using the larger instrument. Under low resolution, some of the P(J) laser pulses in Figures 5, 6, and 7, for example 1-0 P(7) (Fig. 6), would appear to have two time-resolved peaks, whereas in fact the second pulse was the time-delayed  $\text{H}^{37}\text{Cl}$  peak.

Lasing from  $\text{H}^{37}\text{Cl}$  2-1 and 1-0 transitions affects the laser pulse shape as can be seen in Figure 8, where a composite laser pulse has been constructed from the data of Figure 6. The agreement with the experimental pulse shape (Figure 4(b)) is quite good.

As a result of the relative isotopic abundance of  $^{35}\text{Cl}$  and  $^{37}\text{Cl}$ , the inherent gain of an  $\text{H}^{37}\text{Cl}$  line is one-third that of the same  $\text{H}^{35}\text{Cl}$  vibrational-rotational transition. Therefore, certain  $\text{H}^{37}\text{Cl}$  transitions were completely missing, even though the corresponding  $\text{H}^{35}\text{Cl}$  transitions were observed. The observed  $\text{H}^{37}\text{Cl}$  transitions had a longer time-to-threshold and approximately one-third lower intensity than the identical transitions in  $\text{H}^{35}\text{Cl}$ .

Since the  $\text{H}^{37}\text{Cl}$  transitions had lower gain and required longer time to reach threshold, the upper vibrational levels were much more sensitive to the chemical pumping reactions and vibrational decay process. Therefore,



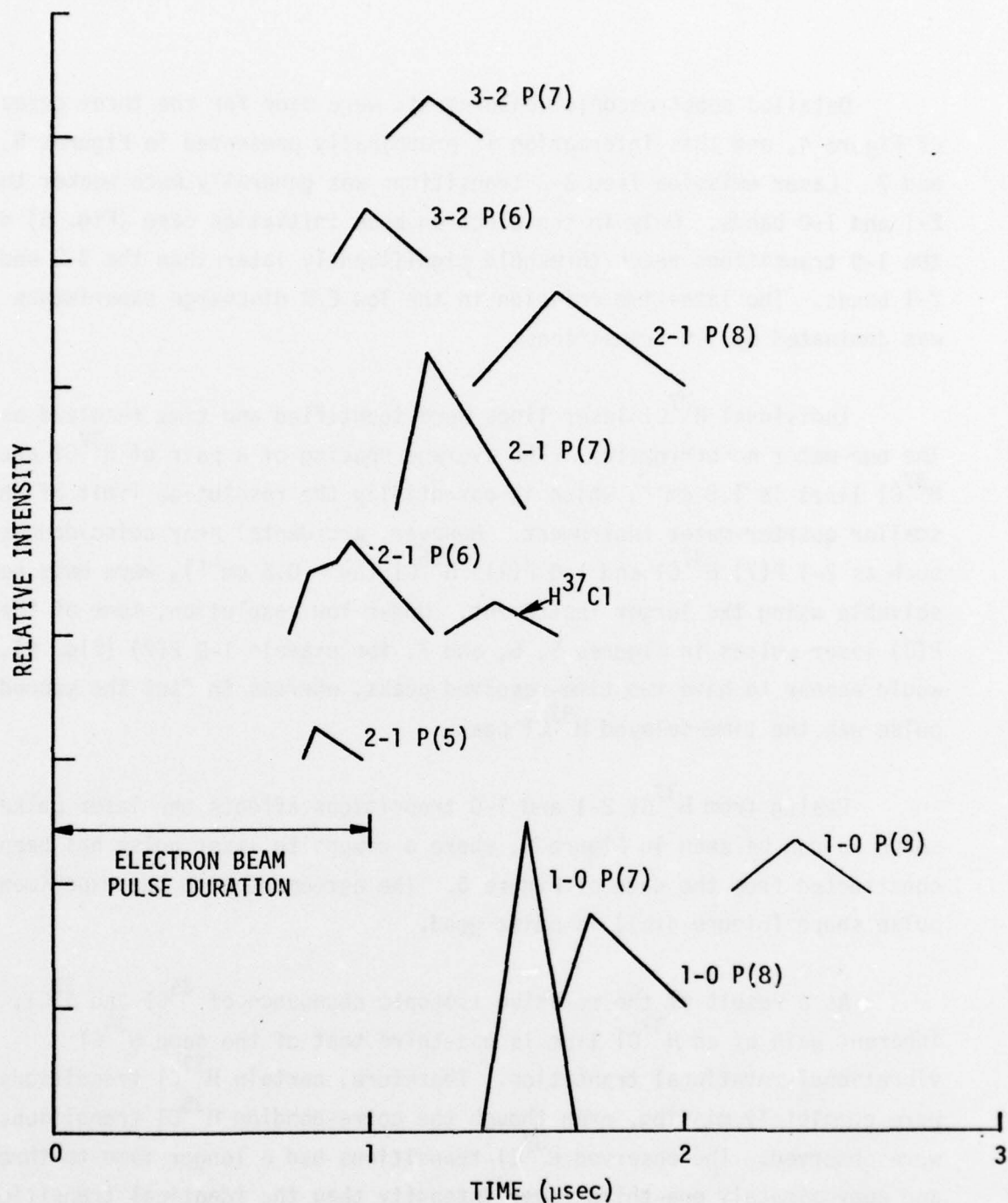


Figure 5. Time Histories and Relative Intensities of the HCl Laser Transitions Observed Using Only the Electron Beam for Excitation. Gas pressure was 400 torr and the gas mixture was Ar/H<sub>2</sub>/Cl<sub>2</sub> (49/49/2).

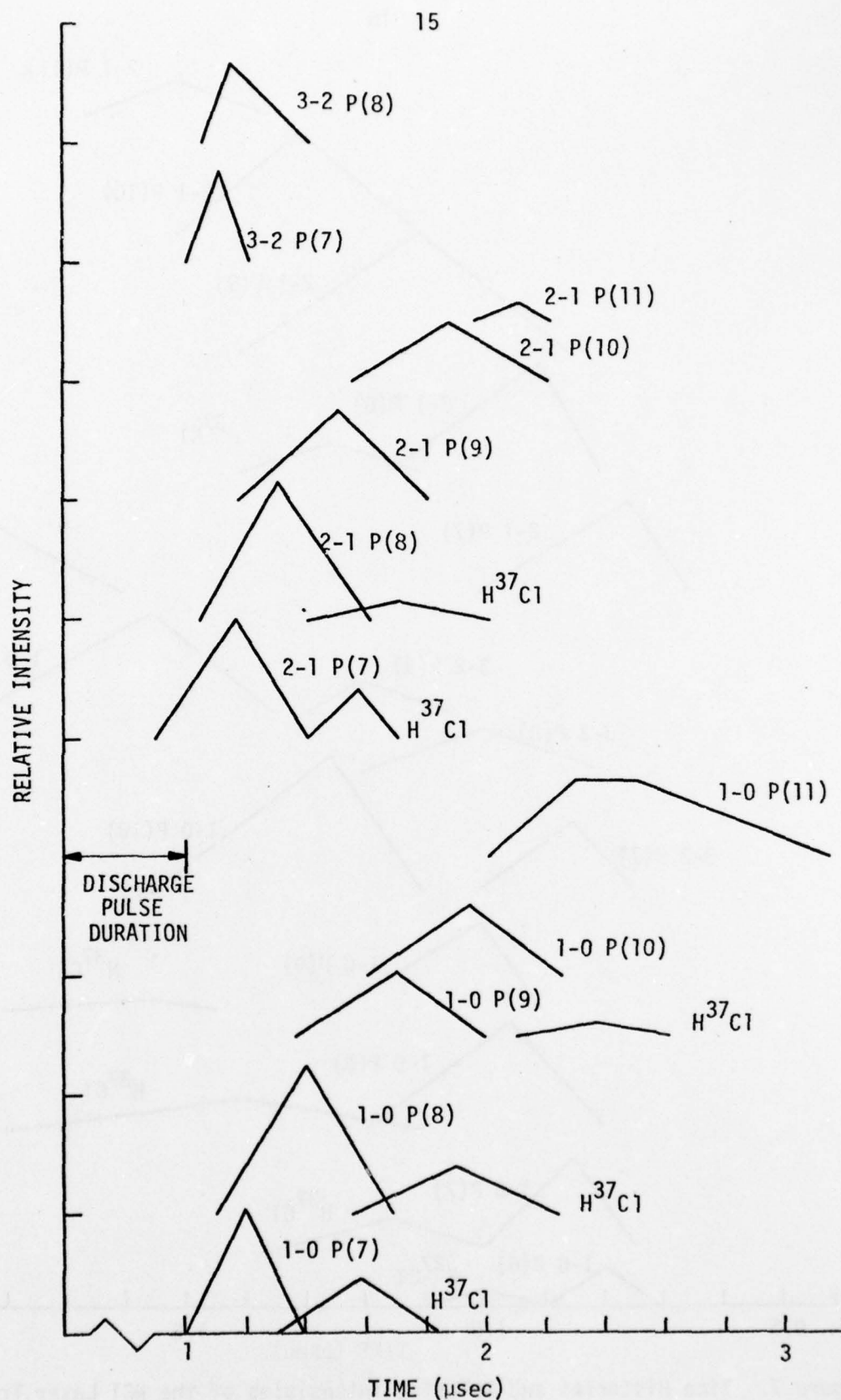


Figure 6. Time Histories and Relative Intensities of the HCl Laser Transitions Observed in Low E/N ( $1.55 \times 10^{-16}$  V-cm<sup>2</sup>) Discharge Excitation. Gas pressure was 400 torr and the gas mixture was Ar/H<sub>2</sub>/Cl<sub>2</sub> (49/49/2).

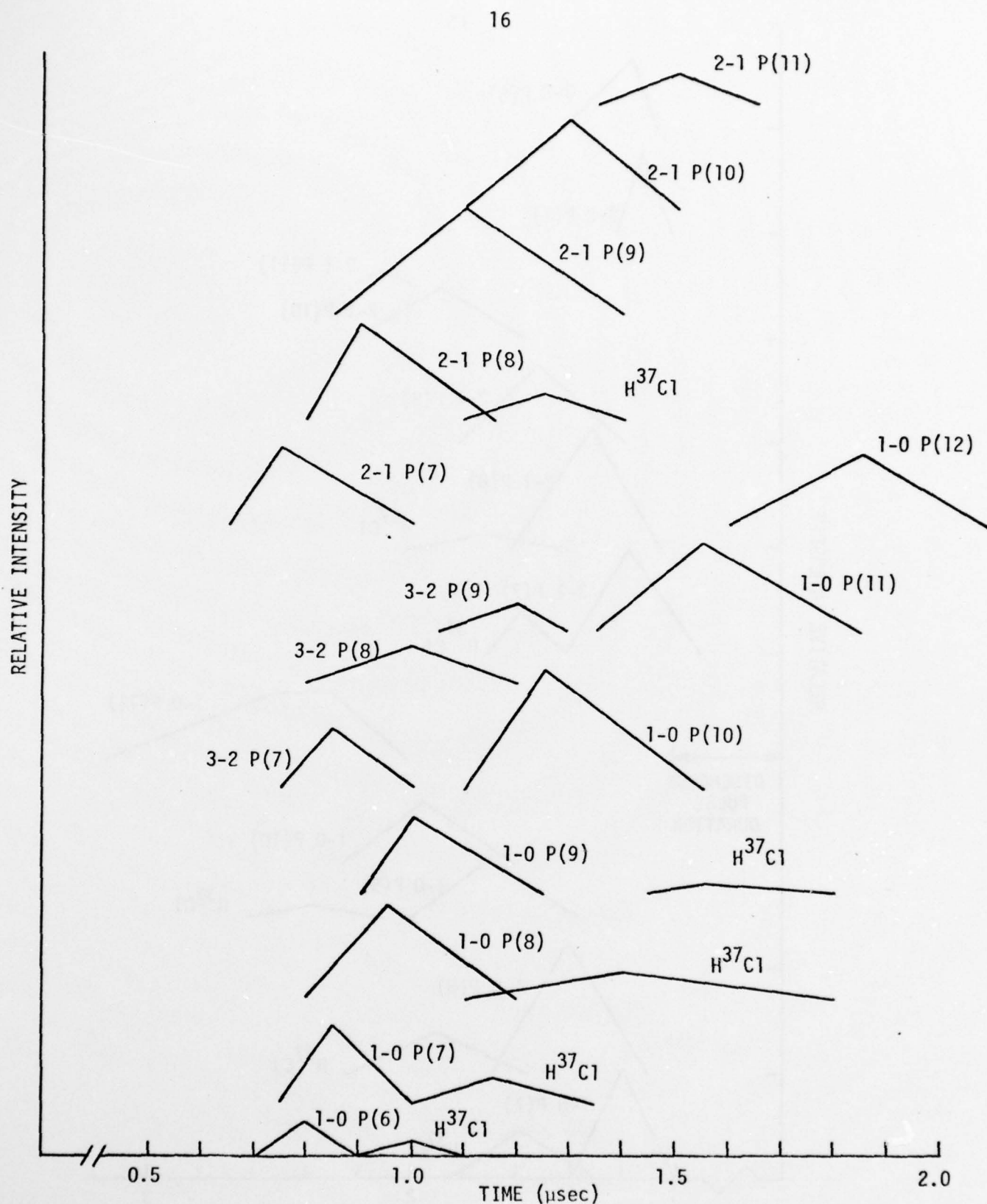


Figure 7. Time Histories and Relative Intensities of the HCl Laser Transitions Observed in High  $E/N$  ( $2.5 \times 10^{-16}$  V-cm<sup>2</sup>) Discharge Excitation. Gas pressure was 400 torr and the gas mixture was Ar/H<sub>2</sub>/Cl<sub>2</sub> (49/49/2).

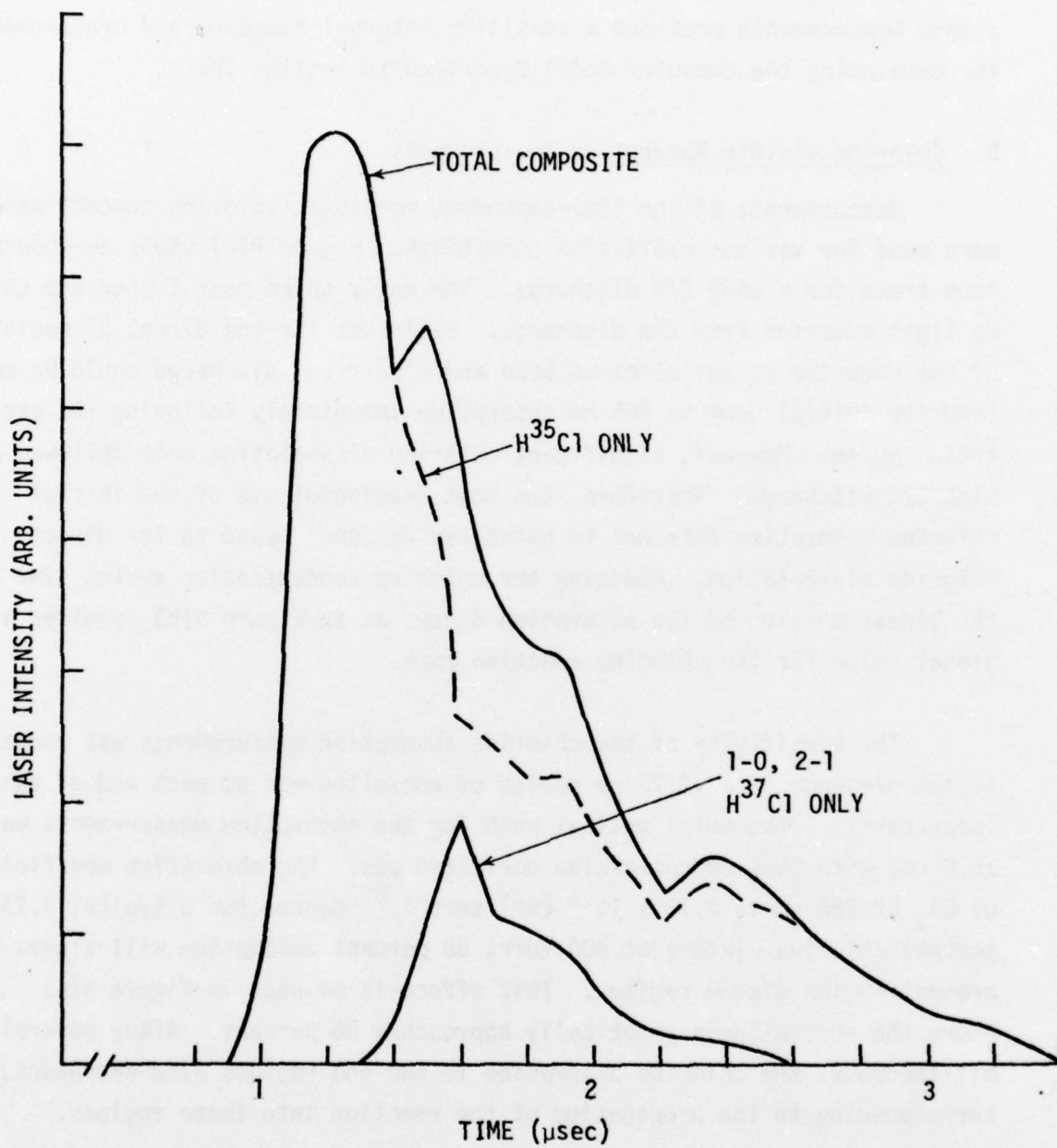


Figure 8. Reconstructed HCl Laser Pulse Shape Using the Low E/N Discharge Data Presented in Figure 6



the information obtained from the time-resolved  $\text{H}^{37}\text{Cl}$  and  $\text{H}^{35}\text{Cl}$  spectroscopic measurements provided a sensitive internal standard and cross-check for developing the computer model described in Section IV.

#### B. Chlorine Visible Absorption Measurements

Measurements of the time-dependent molecular chlorine concentration were made for various excitation conditions. Figure 9(a) shows an absorption trace for a high E/N discharge. The early spike near 1  $\mu\text{sec}$  was caused by light emission from the discharge. Estimates for the direct dissociation of the chlorine by the electron beam and electrical discharge could be made from the initial drop in 365 nm absorption immediately following the excitation pulse. However, significant chlorine dissociation only followed a high E/N discharge. Therefore, the most meaningful use of the initial chlorine absorption data was to establish an upper bound to the direct chlorine dissociation. Plotting the chlorine concentration versus time for the linear portion of the absorption decay, as in Figure 9(b), yielded a global value for the chlorine reaction rate.

The sensitivity of the chlorine absorption measurements was reduced by the presence of a 12.75 cm region of unexcited gas at each end of the laser cavity. The total optical path for the absorption measurements was 75.5 cm, with 25.5 cm containing unexcited gas. The absorption coefficient of  $\text{Cl}_2$  at 365 nm is  $3.73 \times 10^{-3} \text{ cm}^{-1} \text{ torr}^{-1}$ .<sup>6</sup> Hence, for a typical 1.75 percent chlorine mixture at 400 torr, 50 percent absorption will always be present in the window regions. This effect is evident in Figure 9(a) where the absorption asymptotically approaches 50 percent. After several milliseconds, the chlorine absorption in the end regions also decreases, corresponding to the propagation of the reaction into these regions.

#### C. Laser Energy Measurements

Parametric laser energy measurements were made for a variety of gas mixtures and discharge conditions. Figure 10 shows the laser energy as a

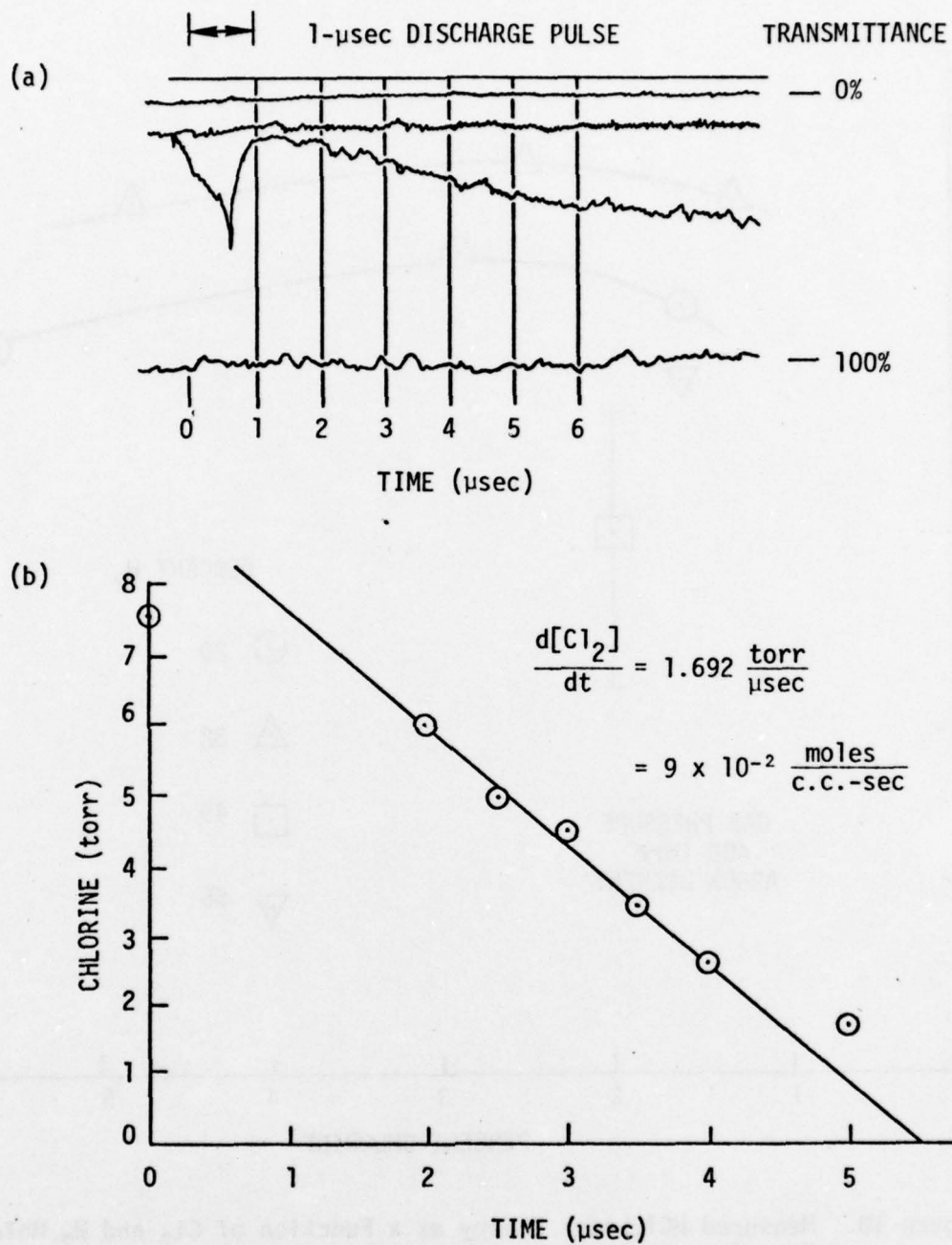


Figure 9. Rate of Chlorine Disappearance in the High E/N ( $2.5 \times 10^{-16}$  V-cm<sup>2</sup>) Discharge. Gas pressure was 400 torr and the mixture was Ar/H<sub>2</sub>/Cl<sub>2</sub> (49/49/2).

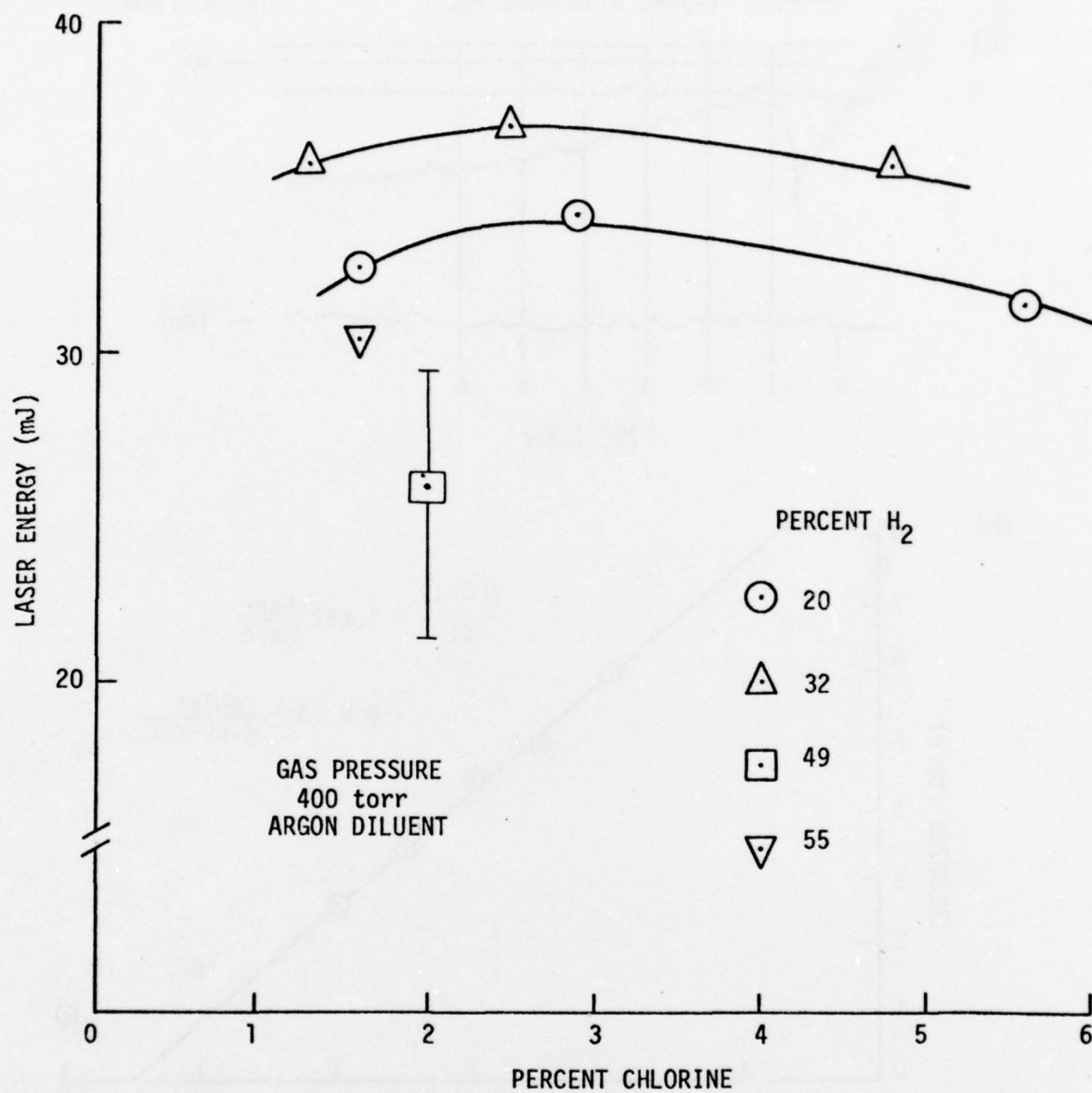


Figure 10. Measured HCl Laser Energy as a Function of Cl<sub>2</sub> and H<sub>2</sub> Mole Fractions Using Electron Beam Excitation

function of hydrogen and chlorine concentrations using only the electron beam to initiate the chemical laser. The laser output was fairly insensitive to the chlorine and hydrogen concentrations over the range shown in Figure 10. However, Figure 11 shows that for a constant discharge energy input and  $E/N$ , there is a strong dependence of the laser energy on the chlorine fraction. The energy input to the discharge was kept constant by attenuating the electron beam current, hence maintaining constant discharge current, as the chlorine fraction was reduced. This adjustment in the electron beam current is necessary because of the large ( $\sim 10^{-10} \text{ cm}^3/\text{sec}$ ) electron attachment rate of the chlorine molecule. The laser energy using only the electron beam for excitation is also shown in Figure 11. In contrast to Figure 10, the electron beam current is not the same for each chlorine fraction studied.

The highest electrical efficiency obtained was 4.5 percent in a high  $\text{Cl}_2$  mole fraction (3.5 percent) mixture as shown in Figure 11. Table 2 summarizes the laser output energy and electrical efficiency for the excitation conditions shown in Figure 4. The laser energy was approximately ten times higher using the discharge than it was using the electron beam alone. Higher  $E/N$  discharges would produce more H atoms (see Sec. IV) which would improve the laser output by accelerating the rate of reaction (1) (Table 1) but reduce the electrical efficiency. The quantum efficiency of producing an H atom is at best 10 percent, based on a 9-eV  $\text{H}_2$  dissociation energy and assuming production of  $\text{HCl}$  ( $v=2$ ), and ignoring V-T deactivation.

As expected for a laser system which is strongly dominated by V-T loss mechanisms, the input energy pulse duration plays a crucial role. The cold cathode electron gun and discharge could be operated at excitation pulse lengths as long as 15  $\mu\text{sec}$  or as short as several hundred nsec. In the course of early studies, it was found that by decreasing the pulse duration from 10 to 5  $\mu\text{sec}$ , for the same total electrical energy input, the laser energy doubled. These findings led to the intensive studies conducted with the 1- $\mu\text{sec}$  excitation pulse configuration. For pulse durations less than 1  $\mu\text{sec}$ , the laser energy scaled directly with the energy input pulse length.



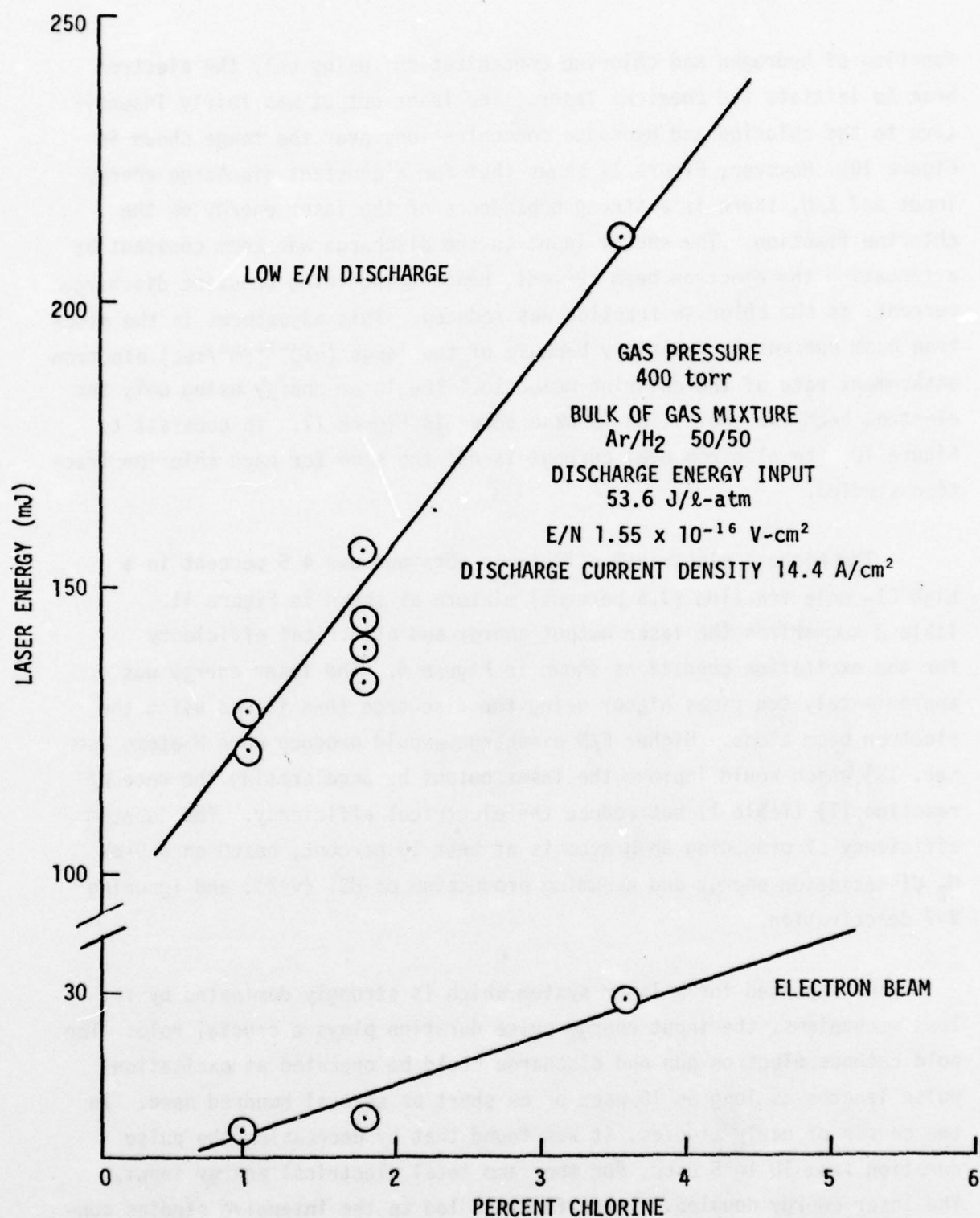


Figure 11. Measured HCl Laser Energy as a Function of Cl<sub>2</sub> Mole Fraction Using Discharge Excitation at Constant Energy Input.

Table 2  
Summary of Laser Output Energies and Electrical Efficiencies

Excitation <sup>1</sup> Conditions	Laser <sup>2</sup> Energy (mJ)	Electrical <sup>3</sup> Energy Input (J)	Electrical Efficiency (%)	Chemical <sup>4</sup> Efficiency (%)
Electron Beam <sup>5</sup> (1 $\mu$ sec pulse) 3.5 A/cm <sup>2</sup>	20 - 30	1.2	~ 2.0	~ 0.2
Electron Beam + Low ( $1.6 \times 10^{-16}$ V-cm <sup>2</sup> ) E/N Discharge (1 $\mu$ sec pulse)	200 - 230	8.1	~ 2.6	~ 1.9
Electron Beam + High ( $2.5 \times 10^{-16}$ V-cm <sup>2</sup> ) E/N Discharge (1 $\mu$ sec pulse)	244 - 260	12.6	~ 2	~ 2.2

<sup>1</sup>Gas mixture Ar/H<sub>2</sub>/Cl<sub>2</sub> (49/49/2) at 400 torr.

<sup>2</sup>A range of laser energies is given which covers identical discharge conditions, data taken on different days.

<sup>3</sup>162 cm<sup>3</sup> active volume was viewed by laser optics.

<sup>4</sup>Based on 44 kcal/mole of Cl<sub>2</sub> present.

<sup>5</sup>The ion pair production rate corresponding to 3.5 A/cm<sup>2</sup> delivered by the electron gun was  $1.6 \times 10^{21}$  sec<sup>-1</sup> and 28 eV per ion pair was deposited in the gas.

## SECTION IV

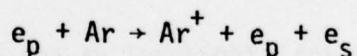
### COMPUTER MODEL DESCRIPTION AND COMPARISONS WITH EXPERIMENT

The computer model was divided into two independent calculations. Purely discharge and electron impact-related phenomena, such as vibrational excitation of hydrogen, were treated in a Boltzmann calculation of the electron distribution function. The second set of calculations dealt with the reaction kinetics and laser gain and used the fractional distribution of electron beam and discharge energy into various molecular excitation channels as input data. Subsections A and B describe the essentials of the electron excitation calculations and the overall features of the chemical kinetics and laser gain program. A set of chemical rate constants and values for the fractional distribution of electrical energy input were found which provided good agreement with the experimentally measured laser and kinetic properties. These parameters will be discussed in Subsection C.

#### A. Analytical Model of Electron Beam and Electric Discharge Physics

##### e-Beam Physics

The production rate,  $S$ , of secondary electrons from the high-energy primary electrons (160 keV),



can be determined from the e-beam current density, mass density, effective ionization energy, and primary electron energy loss rate for each species of the gas mixture. Effective ionization energies for  $\text{H}_2$  and Ar were obtained from Whyte,<sup>7</sup> and the electron energy loss rates were obtained from Berger and Seltzer.<sup>8</sup> It has recently been demonstrated by Searles and Hart<sup>9-11</sup> that the energy deposition rates calculated using the Berger and Seltzer tables are two to four times smaller than that obtained from calculations

which consider scattering of the incident high energy electrons by the foil and multiple scattering in the gas. Hence, the ion-pair production rate  $S$  calculated using the Berger and Seltzer tables ( $8 \times 10^{20}/\text{cm}^3\text{-sec}$ ) for the standard gas mixture studied, 49% Ar, 49%  $\text{H}_2$ , 2%  $\text{Cl}_2$ , was multiplied by 2 to yield  $1.6 \times 10^{21}/\text{cm}^3\text{-sec}$ . This value of the ion-pair production rate was found to be consistent with the observed discharge current and atom (H and Cl) production rates, as will be discussed below.

Because of the large electron attachment rate coefficient for  $\text{Cl}_2$ , the total attachment rate can be equated to the ion-pair production rate and dissociative recombination processes can be ignored. Hence, the observed discharge current only depends upon the electron drift velocity and attachment rate coefficient. For  $\text{Cl}_2$ , the published thermal electron attachment rate constants range from  $3 \times 10^{-10}$ <sup>(12)</sup> to  $3.7 \times 10^{-9}$ <sup>(13)</sup>  $\text{cm}^3/\text{molecule-sec}$ . Very little information<sup>14</sup> exists on the electron energy dependence (above 0.25 eV) of the rate coefficient. From the present measurements of the discharge current density ( $24 \text{ A/cm}^2$ ) in low  $E/N$  ( $1.6 \times 10^{-16} \text{ V-cm}^2$ ) discharges, in  $\text{Ar/H}_2/\text{Cl}_2$  (49/49/2) mixtures, an electron attachment rate coefficient of  $1.5 \times 10^{-10} \text{ cm}^3/\text{molecule-sec}$  for  $\text{Cl}_2$  has been found using a calculated drift velocity of  $3.3 \times 10^6 \text{ cm/sec}$ . The procedure for calculating the drift velocity will be outlined in the discharge physics section below.

Some elementary time-dependent computer calculations were made for the electron detachment process  $\text{H} + \text{Cl}^- \rightarrow \text{HCl} + \text{e}$ , using the published<sup>15</sup> rate constant ( $9 \times 10^{-10} \text{ cm}^3/\text{molecule-sec}$ ) for this reaction. In the absence of the detachment reaction, the electron density reached the steady state value ( $3 \times 10^{13}/\text{cm}^3$ ) early in the pulse (100 nsec), but then decayed to half this value by the end of the 1  $\mu\text{sec}$  pulse. The inclusion of the H-atom detachment reaction prevented the decay of the electron density over the entire pulse duration. However, the H atom reaction did not significantly affect the overall magnitude of the electron density, which was still strongly determined by the  $\text{Cl}_2$  attachment rate coefficient.



### Discharge Physics

In the presence of an electric field, it is necessary to solve the Boltzmann equation for the electron distribution function in order to obtain the drift velocity, mean electron temperature, and excitation rates for the various electron impact inelastic collision processes involved.

For a given gas mixture and applied electric field normalized by the gas density ( $E/N$ ), the Boltzmann transport equation can be solved if the elastic and inelastic electron-impact cross sections are known as a function of electron energy. These cross sections are well known for the dominant gases,  $H_2$  and Ar, in the gas mixture under study but are not available for  $Cl_2$  (except for the dissociative attachment process).

Cross sections for argon were obtained from Engelhardt and Phelps.<sup>16</sup> For hydrogen, the momentum transfer cross section came from Gibson,<sup>17</sup> the rotational and vibrational excitation cross section from Linder and Schmidt,<sup>18</sup> and the dissociation cross section from Chun, Lin and Lee.<sup>19</sup> The drift velocity and characteristic electron energy are shown as a function of  $E/N$  in Figure 12 for a 50%  $H_2$ -50% Ar mixture. Fractional electrical power distribution as a function of  $E/N$  is shown in Figure 13.

A check on the self-consistency of the model for both e-beam and discharge properties was made by comparing the experimentally measured discharge current with that given theoretically. The electron density was calculated by equating the ion-pair production rate and the  $Cl_2$ -dominated electron attachment rate ( $S = \beta N_e N_{Cl_2}$ ). The electron drift velocity was obtained from the Boltzmann code calculations. The discharge current was then found by the product of electron density, drift velocity and electron charge. The agreement was generally within 10 to 20 percent, which is quite satisfactory.

Since data for the electron impact dissociation cross section of  $Cl_2$  was not available, parametric values for the fraction of discharge energy entering  $Cl_2$  dissociation were tried. It was found that only 10 percent

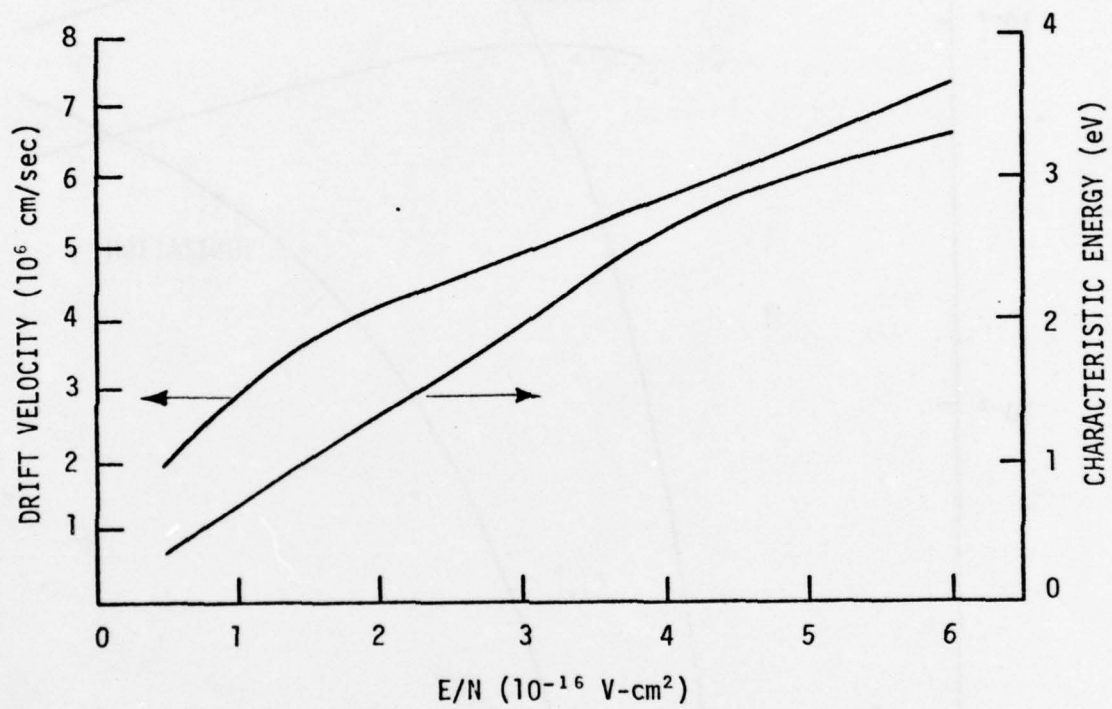


Figure 12. Drift Velocity and Characteristic Electron Energy for an  $\text{Ar}/\text{H}_2$  Mixture

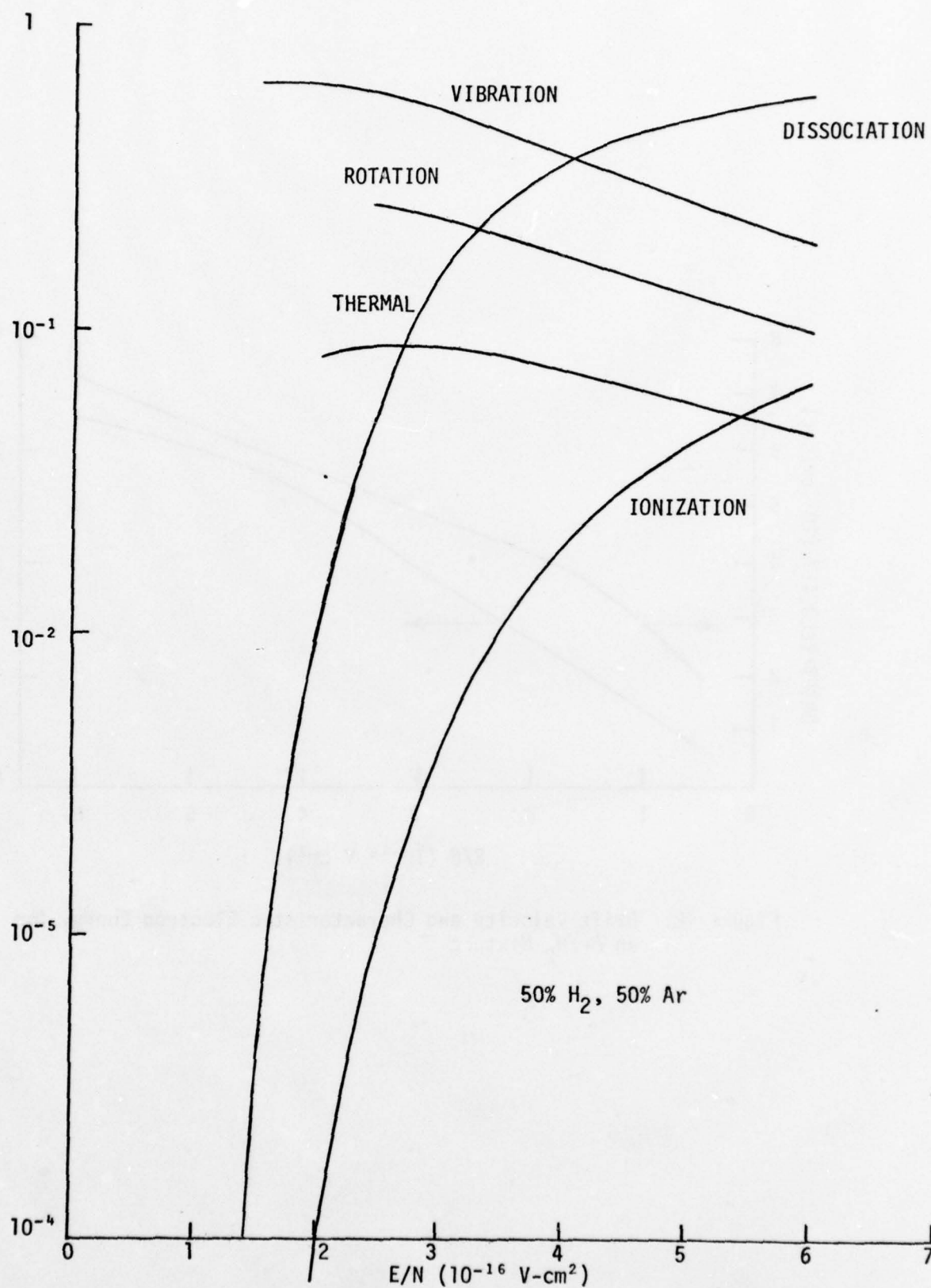


Figure 13. Boltzmann Calculations for an Ar/H<sub>2</sub> (50/50) Mixture

77 00770

or less of the discharge energy needed to be placed in  $\text{Cl}_2$  dissociation to give good agreement with the observed  $\text{Cl}_2$  burn rate and laser properties discussed in Section II. This implies 4.5 percent dissociation of the  $\text{Cl}_2$  by the discharge ( $E/N = 1.6 \times 10^{-16} \text{ V-cm}^2$ ). For comparison purposes, 1%  $\text{F}_2$  dissociation has been measured<sup>20</sup> for an electron beam-stabilized discharge in mixtures of  $\text{He}/\text{H}_2/\text{F}_2$ . Reference 20 also proposes a mechanism involving heating of  $\text{F}^-$  ions, by the discharge field, to temperatures of the order of 1 eV. At this energy, the electron can rapidly detach from  $\text{F}^-$  in heavy particle collisions, and the electron is quickly lost again to dissociative attachment to  $\text{F}_2$ . A chain length of 3.5 is proposed in Reference 20 for this process. This reaction was not included in the simple plasma model of the previous section; however, if it were included, a larger value of the chlorine dissociative attachment rate could be used along with a correspondingly smaller dissociation fraction by the discharge. These changes would be small, less than factors of 3 to 4 in the calculated dissociative attachment rate.

#### B. Chemical Kinetics and Laser Gain Computer Model

The kinetic model included only the first four HCl vibrational energy levels ( $v=0,1,2,3$ ). Only single quantum energy exchange and deactivation processes were considered. HCl V-V ladder climbing processes were limited to  $\text{HCl } (v=1) + \text{HCl } (v') \rightleftharpoons (v'+1) + \text{HCl } (0)$  with a partially reflecting boundary for  $v' = 3$ , i.e.,  $\text{HCl } (v=4)$  molecules were considered lost via further V-V processes. The vibrationally excited  $\text{H}_2$  formed by the discharge was assumed to be in a Boltzmann equilibrium and only  $\text{H}_2$  ( $v=0,1$ ) were considered as reacting species.

A recent review of rate constants relevant to the HCl chemical laser system by N. Cohen and J. Bott<sup>21</sup> was extremely useful in summarizing and providing a critical review of the literature. These data were supplemented by more recent data appearing after the publication of Reference 21. Table 3 summarizes the rate coefficients for the chemical reactions and deactivation processes included in the model.



Table 3  
Rate Coefficients for the HCl Chemical Laser System

Reaction	Rate Coefficient (c.c./mole-sec)	Comments/Reference
$H + Cl_2 \rightarrow HCl(v) + Cl$	$K = 9.98 \times 10^{13} T^{-0.163} e^{-1268/T} \cdot f(v)$ $f(0) = 0, f(1) = 0.12, f(2) = 0.46$ $f(3) = 0.42$	1.75 times faster than the rate recommended by Reference 21. Vibrational fractions Reference 22.
$Cl + H_2(v) \rightarrow HCl(v') + H$	$K = 9.6 \times 10^{13} e^{-2647/T}$ for $v=v'=0$ $K = 1.3 \times 10^{13} T^{-0.268} e^{-845/T}$ for $v=1, v'=0$ $K = 2.8 \times 10^{14} T^{-0.536} e^{-990/T}$ for $v=v'=1$	2 times faster than the rate recommended by Reference 21. 1/10 the rates calculated in Reference 5.
$HCl(v) + HCl(v') \rightarrow HCl(v+1) + HCl(v'-1)$	$K = 9 \times 10^{14}/T$ $v=v'=1$ $K = 36 \times 10^{14}/T$ $v=1, v'=2$ $K = 27 \times 10^{14}/T$ $v=1, v'=3$	Reference 23 gave rate constant for $T = 300^\circ K$ , temperature dependence used was suggested by Reference 21. Scaling with $v'$ derived from present work.
$HCl(v) + HCl \rightarrow HCl(v-1) + HCl$	$K = (1.6 \times 10^{17} T^{-3} + 8.7 \times 10^{14} T^2) v$	Reference 24 studied the temperature dependence in the range of interest; deactivation by levels other than $HCl(0)$ are assumed equal to the rate derived for $HCl(0)$

Table 3 (Cont'd.)

Reaction	Rate Coefficient (c.c./mole-sec)	Comments/Reference
$\text{HCl}(v)+\text{H}_2 \rightarrow$ $\text{HCl}(v-1)+\text{H}_2$	$v(1 \times 10^4 T^{2.23})$	Suggested $v$ and $T$ scaling of Reference 21, based on $v = 1$ and $T = 300^\circ\text{K}$ data of References 25 and 26.
$\text{HCl}(v)+\text{Cl}_2 \rightarrow$ $\text{HCl}(0)+\text{Cl}_2$	$4 \times 10^9$	This deactivation rate was omitted from the calculation because of the low $\text{Cl}_2$ (1-2%) concentration and slow rate measured in Reference 26.
$\text{HCl}(v)+\text{Ar} \rightarrow$ $\text{HCl}(v-1)+\text{Ar}$	$2.8 \times 10^7$	This deactivation rate (Ref. 27) was omitted from the calculation since it is two orders of magnitude smaller than the $\text{HCl}(v)+\text{H}_2$ rate.
$\text{HCl}(v)+\text{H} \rightarrow$ $\text{HCl}(v-1)+\text{H}$	$4 \times 10^{12}$ $v = 1$ $8 \times 10^{12}$ $v = 2$ $9 \times 10^{12}$ $v = 3$	References 28 and 29 generally agree on the value for $v = 1$ . The rates for $v = 2, 3$ were based on the present work and Ref. 30.
$\text{HCl}(v)+\text{Cl} \rightarrow$ $\text{HCl}(v-1)+\text{Cl}$	$4.8 \times 10^{13} e^{-693/T}$ $v = 1$ $2.1 \times 10^{14} e^{-693/T}$ $v = 2$ $4.2 \times 10^{14} e^{-693/T}$ $v = 3$	Reference 31 measured the temperature dependence for $v = 1$ , and Reference 30 gave data for $v = 2$ and the rate for $v = 3$ was based on the present work. The temperature dependence for $v = 2$ and 3 were assumed equal to that found for $v = 1$ .
$\text{H}_2(v=1)+\text{H} \rightarrow \text{H}_2(v=0)+\text{H}$	$2 \times 10^{11}$	Reference 32.

The kinetic master equation included all the reactant and product species and the HCl and H<sub>2</sub> vibrational level populations within the limitations discussed above. In the case of stimulated emission, there exists an additional set of coupled equations for the HCl laser transitions which are included in determining the vibrational level populations. These kinetic and laser equations were solved simultaneously with the energy conservation equation using the Runge-Kutta-Gill method of integration.

Calculations for H<sup>35</sup>Cl and H<sup>37</sup>Cl were run separately using a constant (0.75 or 0.25) in the kinetics model which represents the fractional isotopic abundance of <sup>35</sup>Cl or <sup>37</sup>Cl. The constant multiplied all production terms for specific vibrational levels in HCl in such a manner that the total HCl concentration still appears as a deactivating species and the correct chlorine atom and molecule densities were computed.

The model does not include V-V exchange between H<sup>35</sup>Cl and H<sup>37</sup>Cl. The exchange rate reported by Leone and Moore<sup>23</sup> ( $1.1 \times 10^{13}$  cm<sup>3</sup>/mole-sec) implies a V-V time of 10 to 100  $\mu$ sec for HCl densities on the order of  $10^{-9}$  to  $10^{-8}$  moles/cc. Hence, for the range of HCl ( $v=0,1$ ) densities found in the model, the rate of isotopic V-V exchange is slow on the time scale of interest.

In order to calculate the laser flux from an optical cavity, it is necessary to know the gain coefficient of the amplifying medium. For the experimental condition of this study, the gain coefficient is fully pressure broadened and is given for the P-branch ( $J-1 \rightarrow J$ ) by

$$g_{UL} = \frac{\lambda_{UL}^2}{4\pi^2} \frac{A_{UL}}{\Delta\nu_c} \frac{B_U}{T_r} (2J-1) e^{-[J(J-1)B_U]/T_r} \left\{ 1 - \frac{n_L}{n_U} \frac{B_L}{B_U} e^{-[J(J+1)B_U + J(J-1)B_L]/T_r} \right\} n_U$$

where

$\lambda_{UL}$  = transition line center wavelength

$A_{UL}$  = spontaneous transition probability

$B_U, B_L$  = characteristic rotational constants for upper and lower levels

$n_U, n_L$  = total population of upper and lower vibrational levels, respectively

$T_r$  = rotational temperature

$\Delta\nu_c$  = Lorentz broadened linewidth (full width at half maximum)

$J$  = lower level rotational quantum number

The wavelengths and rotational constants were obtained from G. Herzberg,<sup>33</sup> the transition probabilities from J. M. Herbelin and G. Emanuel,<sup>34</sup> and the Lorentz broadening from H. Babrov et al.<sup>35</sup> The Lorentz broadening of HCl is strongly J-dependent for not only self-broadening but also for H<sub>2</sub> and Ar broadening. Since the experimental data of Reference 36 for H<sub>2</sub> and Ar did not cover all the J values of interest, the broadening had to be extrapolated to the higher J's as shown in Figure 14. For HCl self-broadening, the experimental data of Benedict et al.<sup>37</sup> was used for  $J \leq 13$ ; for larger values of J, the value at P(13) was used since this was essentially the asymptote of  $\Delta\nu_c$  as a function of P(J).

The laser flux in the cavity may be found by integrating the equation for cavity intensity ( $\Phi$ )

$$\frac{d\Phi}{dt} = c\Phi(g - g^{th})(L_{CAV}/L_m)$$

where  $c$  is the speed of light and  $g^{th}$  is the threshold gain (where the cavity gain balances the losses exactly). The final term, which is the ratio



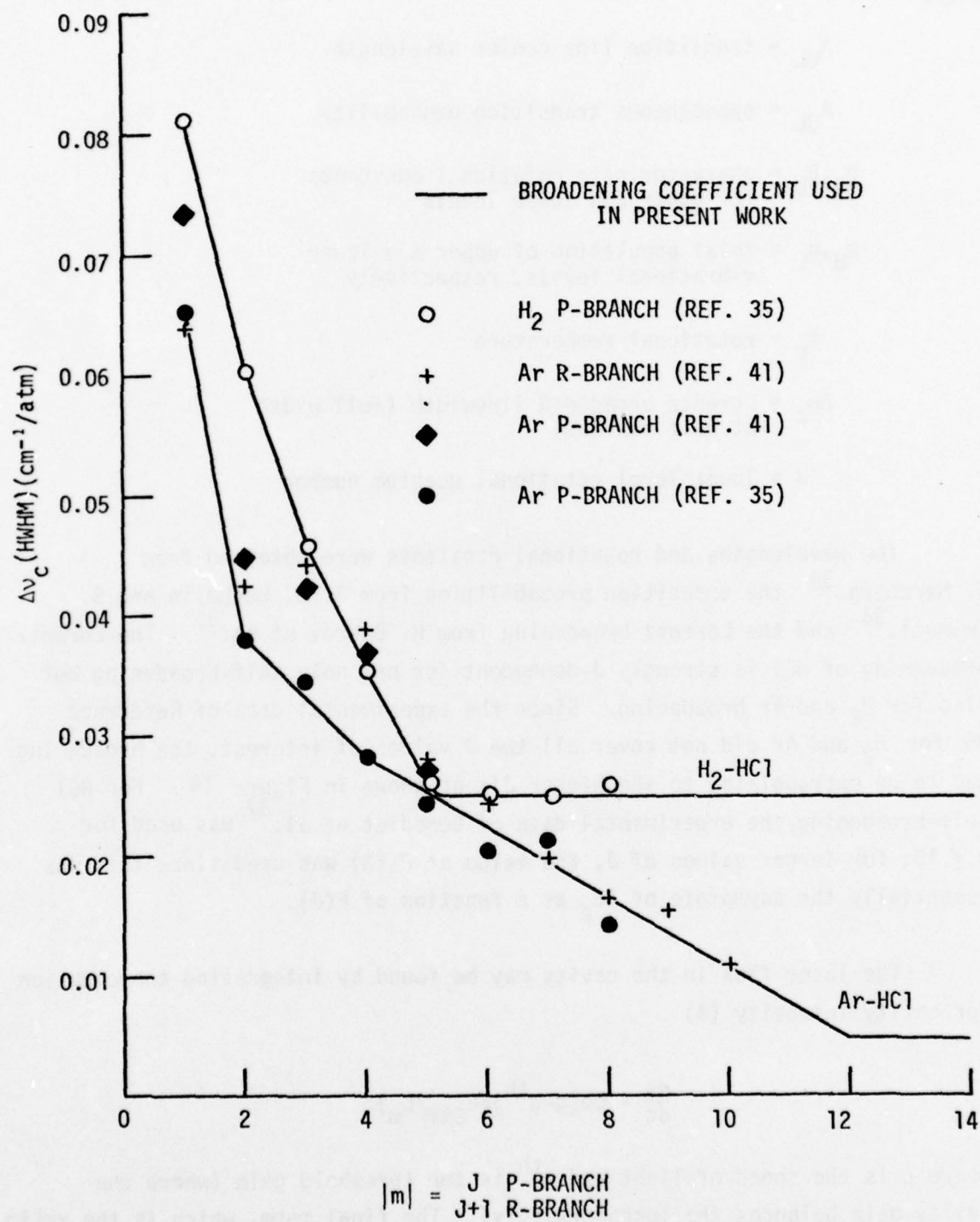


Figure 14. HCl-H<sub>2</sub> and HCl-Ar Optical Broadening Coefficients

of the active medium cavity length (50 cm) to the mirror separation length (130 cm), accounts for the fraction of time the laser mode spends in the active region. In the case of HCl, where several vibrational lines lase simultaneously, a cavity intensity equation was used for each vibrational line. In addition, each vibrational line would have an equation for each rotational line; however, this was simplified by solving only one cavity intensity equation for each vibrational line, with the transition going on the optimum gain, rotational-vibrational transition (i.e., complete rotational equilibrium).

### C. Computer Model Comparisons with Experimental Observations

The electron beam-initiated chemical laser presents the least number of variables for modelling the chemical kinetics. The principal V-T rates for Cl and H atoms on HCl(v) have been measured by several independent groups, and the rates are in good agreement. The V-V rates, at least for  $v = 1$ , for HCl(v) and H<sub>2</sub>(v) are also well established and were not altered in the present calculations.

Four rates were found to be extremely sensitive in analyzing the electron beam-initiated chemical laser. Production rates of H and Cl atoms and the rate constants for the "hot" H+Cl<sub>2</sub> and "cold" Cl+H<sub>2</sub> reactions were investigated in some detail.

The maximum amount of H-atom production was bounded by the energy available from the primary electron beam (~30 eV/ion pair), which implies a maximum of six hydrogen atoms (4.5 eV/H atom) per ion pair. The lower bound on the H-atom production is established by the observed laser energy which was almost directly proportional to the H-atom production rate and the rate constant chosen for the H+Cl<sub>2</sub> reaction. However, as the reaction rate was increased in the model for decreased H-atom production, the overall pulse shape changed. In addition, it was found that good agreement of the model with the discharge experiments could only be obtained by maintaining the H+Cl<sub>2</sub> rate at the value shown in Table 3. This rate coefficient is a factor of 1.75 times larger than the value recommended by Reference 21

and well within the overall spread of experimental results summarized in Reference 21. The H-atom production rate, which was consistent with this choice of rate constant, was 2.25 H-atoms per ion pair. Reference 20 estimates (Eq. A19) that two H-atoms would be produced per ion pair, which is in good agreement with the value derived in the present work.

Laser emission from 2-1  $\text{H}^{37}\text{Cl}$  also established a lower bound to the amount of H-atom present, since its time to threshold was quite sensitive to the H-atom production. If the H-atom production was decreased to one H-atom per ion pair, the calculated 2-1  $\text{H}^{37}\text{Cl}$  threshold time was delayed too long (0.8  $\mu\text{sec}$ ) from the experimentally observed time.

The cold reaction ( $\text{Cl} + \text{H}_2$ ) rate constant listed in Table 3 is a factor of 2 larger than the recommended value of Reference 21. However, a recent<sup>38</sup> reevaluation of this rate constant is within 20 percent of the value used in the present work. The magnitude of this rate coefficient controls the 1-0 laser threshold time since the reaction produces only  $\text{HCl}(0)$ . If the production rate of  $\text{HCl}(0)$  by the cold reaction was reduced, the 1-0 laser transitions reached threshold too early and the pattern of three prominent peaks (Fig. 4(a)) was changed to only two.

For the electron beam-initiated chemical laser, the Cl atom production rate by dissociative attachment would be limited to the ion-pair production rate, whereas it was found that a rate four times higher was required to be consistent with both the experimentally determined burn rate of  $\text{Cl}_2$  and the kinetics of the HCl laser. Therefore, it was assumed that processes similar to the  $\text{H}_2$  dissociation by the e-beam were responsible for producing an additional four chlorine atoms per ion pair. Comparisons of the measured  $\text{Cl}_2$  disappearance rate and the calculated  $\text{Cl}_2$  time-dependent concentration are shown in Figure 15. The measured rate of  $\text{Cl}_2$  consumption, 1 to 2  $\times 10^{-3}$  moles/c.c.-sec, was sensitive to the electron beam pulse length as shown in Figure 15. Independent measurements of the primary

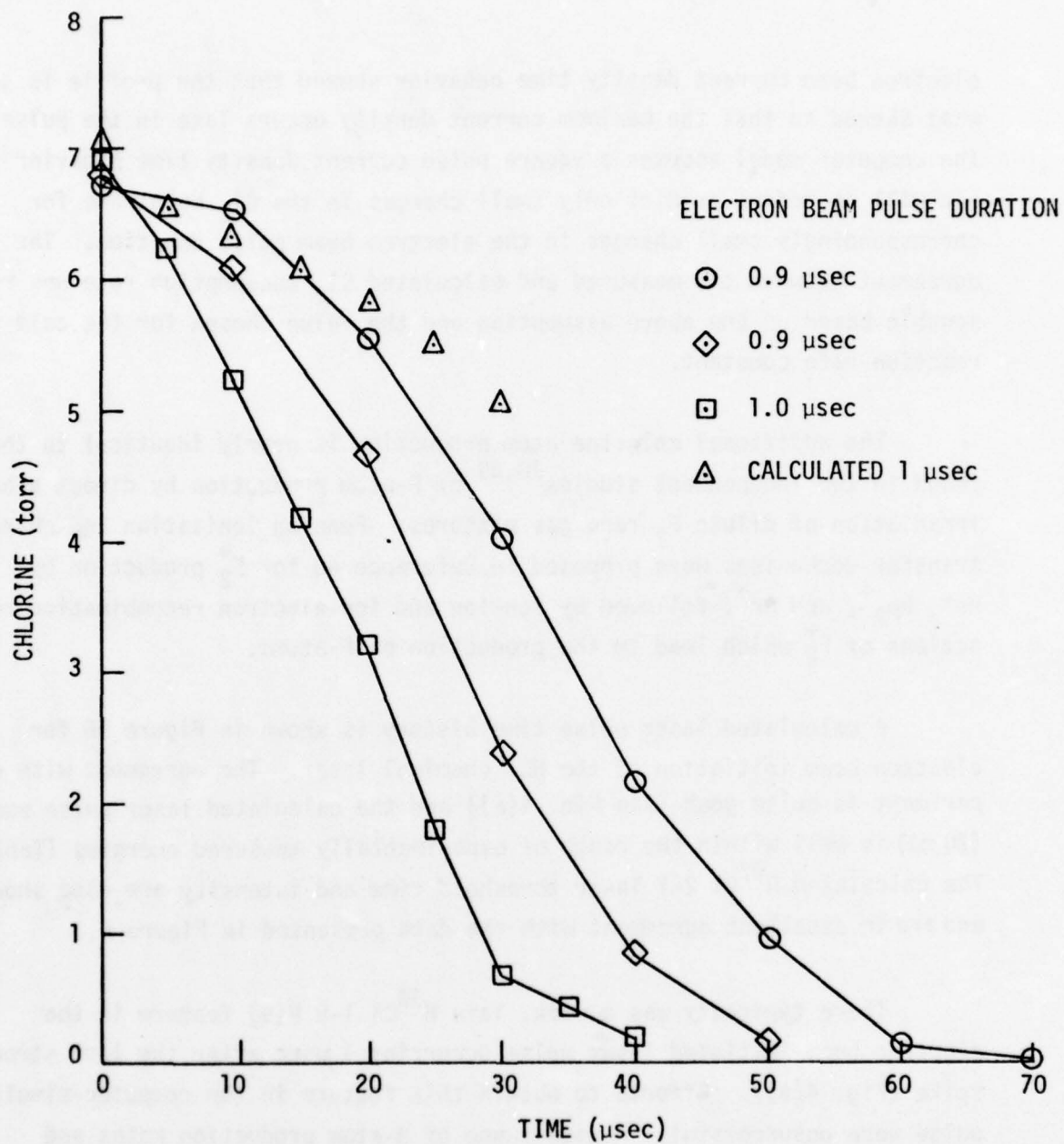


Figure 15. Rate of Chlorine Disappearance Using Only the Electron Beam for Excitation. Gas pressure was 400 torr and the gas mixture was Ar/H<sub>2</sub>/Cl<sub>2</sub> (49/49/2).



electron beam current density time behavior showed that the profile is somewhat skewed so that the maximum current density occurs late in the pulse. The computer model assumes a square pulse current density time behavior and will therefore predict only small changes in the  $\text{Cl}_2$  burn rate for correspondingly small changes in the electron beam pulse duration. The agreement between the measured and calculated  $\text{Cl}_2$  consumption rate was reasonable based on the above assumption and the value chosen for the cold reaction rate constant.

The additional chlorine atom production is nearly identical to that found in two independent studies<sup>20,39</sup> of F-atom production by direct e-beam irradiation of dilute  $\text{F}_2$  rare gas mixtures. Penning ionization and charge transfer mechanisms were proposed in Reference 40 for  $\text{F}_2^+$  production by  $\text{He}^*$ ,  $\text{He}_2^+$ , and  $\text{Ar}^+$ , followed by ion-ion and ion-electron recombination reactions of  $\text{F}_2^+$  which lead to the production of F-atoms.

A calculated laser pulse time history is shown in Figure 16 for electron beam initiation of the HCl chemical laser. The agreement with experiment is quite good (see Fig. 4(a)) and the calculated laser pulse energy (20 mJ) is well within the range of experimentally measured energies (Table 2). The calculated  $\text{H}^{37}\text{Cl}$  2-1 laser threshold time and intensity are also shown and are in excellent agreement with the data presented in Figure 5.

There typically was a weak, late  $\text{H}^{35}\text{Cl}$  1-0 P(9) feature in the electron beam-initiated laser pulse occurring 1  $\mu\text{sec}$  after the last strong spike (Fig. 4(a)). Efforts to obtain this feature in the computer-simulated pulse were unsuccessful. A wide range of H-atom production rates and  $\text{H}+\text{Cl}_2$  reaction rate constants were tried. Nonuniformity of the electron beam spatial distribution was a possible explanation for the late line. Calculations simulating a region of lower e-beam current density showed that essentially only 1-0 transitions lase at approximately 2  $\mu\text{sec}$  after the termination of the electron beam pulse, which is the time at which the

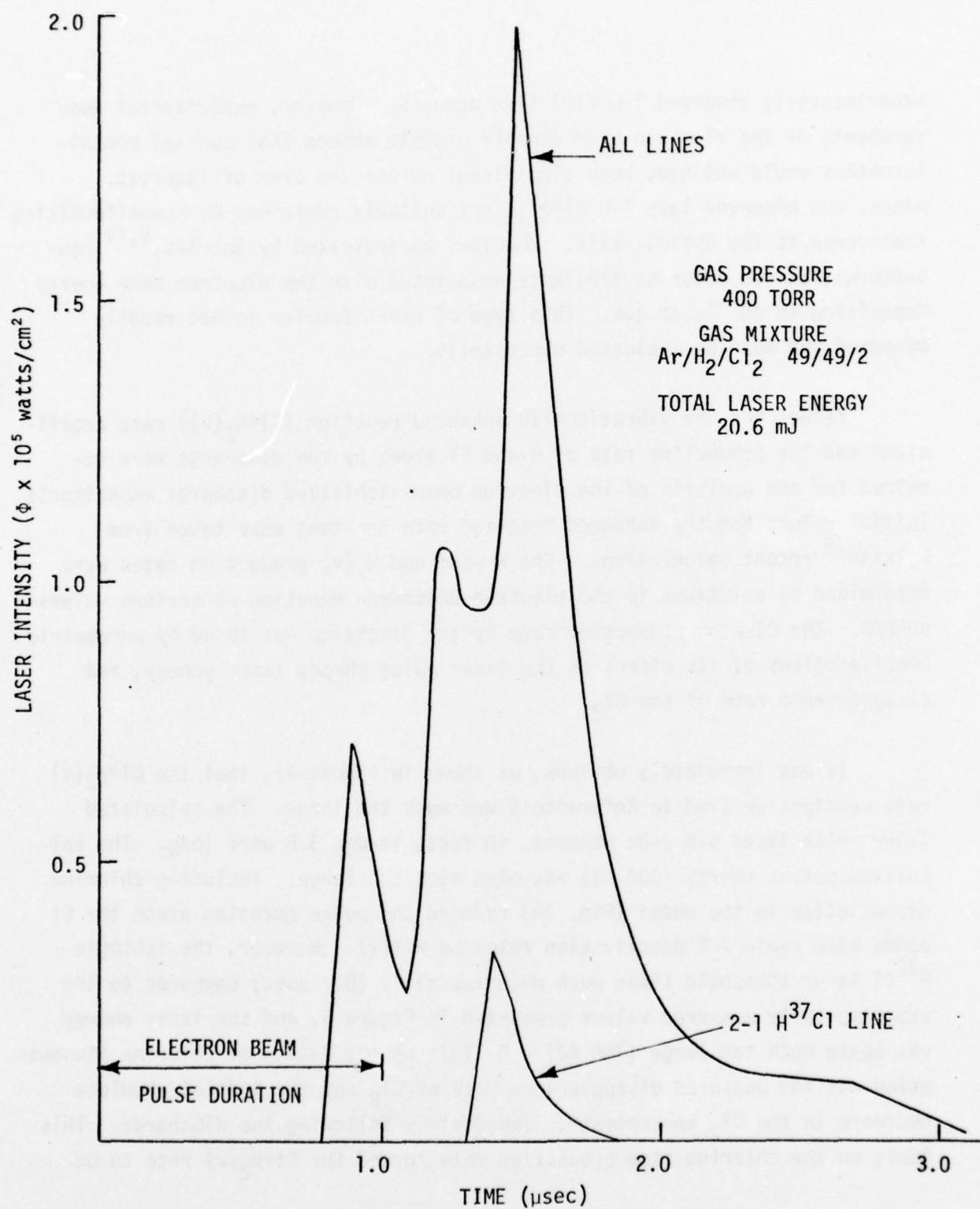


Figure 16. Calculated HCl Chemical Laser Pulse Shape for all Lines and the 2-1  $\text{H}^{37}\text{Cl}$  Line with Electron Beam Excitation

experimentally observed 1-0 P(9) line appears. However, experimental measurements of the electron beam density profile showed that spatial nonuniformities would not have been significant across the area of interest. Hence, the observed late 1-0 P(9) is not suitably explained by nonuniformities transverse to the optical axis. However, as indicated by Searles,<sup>9,11</sup> nonuniformities can occur as gradients associated with the electron beam energy deposition in the laser gas. This type of nonuniformity is not readily measured and must be evaluated numerically.

Values for the vibrationally enhanced reaction ( $\text{Cl} + \text{H}_2(\text{v})$ ) rate coefficient and the production rate of H and Cl atoms by the discharge were required for the analysis of the electron beam-stabilized discharge experiments. Initial values for the enhanced reaction rate constant were taken from Wilkins,<sup>5</sup> recent calculations. The H-atom and  $\text{H}_2(\text{v})$  production rates were determined by solutions to the electron Boltzmann equation at various values of E/N. The Cl-atom production rate by the discharge was found by parametric considerations of its effect on the laser pulse shape, laser energy, and disappearance rate of the  $\text{Cl}_2$ .

It was immediately obvious, as shown in Figure 17, that the  $\text{Cl} + \text{H}_2(\text{v})$  rate constant derived in Reference 5 was much too large. The calculated laser pulse lasts 6.5  $\mu\text{sec}$  whereas, in fact, it was 3.5  $\mu\text{sec}$  long. The calculated output energy (600 mJ) was also much too large. Including chlorine dissociation in the model (Fig. 18) reduced the pulse duration since the Cl atoms have rapid V-T deactivation rates on  $\text{HCl}(\text{v})$ . However, the isotopic  $\text{H}^{37}\text{Cl}$  laser threshold times were much too early (0.7  $\mu\text{sec}$ ) compared to the experimentally measured values presented in Figure 6, and the laser energy was again much too large (750 mJ). A limit on the extent of chlorine dissociation was the measured disappearance rate of  $\text{Cl}_2$  and the initial absolute decrease in the  $\text{Cl}_2$  concentration immediately following the discharge. This limit on the chlorine-atom production rate forced the  $\text{Cl} + \text{H}_2(\text{v})$  rate to be

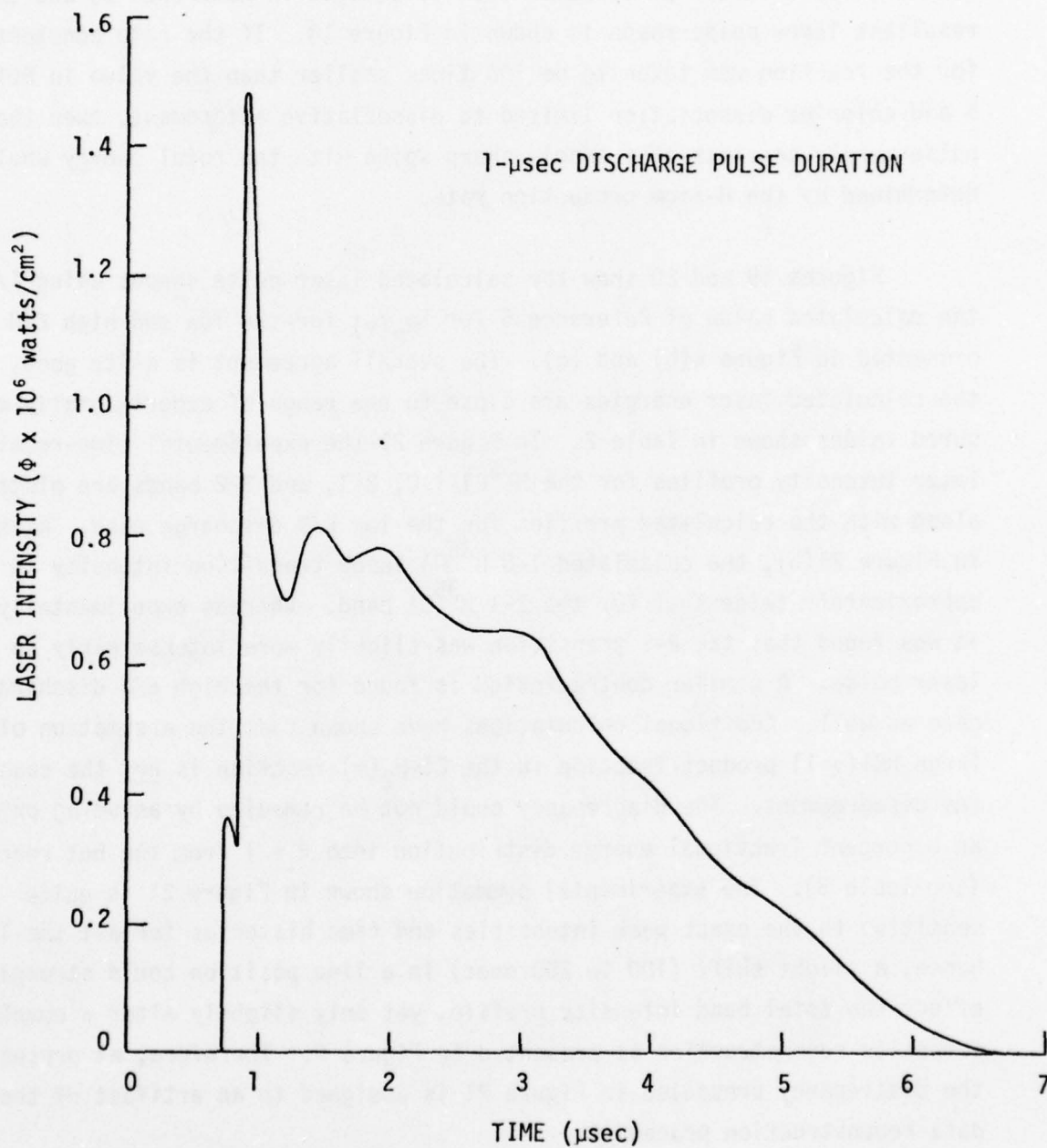


Figure 17. Calculated HCl Laser Pulse Shape for Low E/N ( $1.55 \times 10^{-16}$  V-cm<sup>2</sup>) Discharge Excitation. The rate constant for the vibrationally enhanced reaction was taken from Reference 5, and no chlorine atom production by the discharge was assumed.



decreased by a factor of 10 below that calculated in Reference 5, and the resultant laser pulse shape is shown in Figure 18. If the rate constant for the reaction was taken to be 100 times smaller than the value in Reference 5 and chlorine dissociation limited to dissociative attachment, then the laser pulse merely consists of a single sharp spike with the total energy wholly determined by the H-atom production rate.

Figures 19 and 20 show the calculated laser pulse shapes using 1/10 the calculated value of Reference 5 for  $k_{H_2}(v)$  for the low and high E/N cases presented in Figure 4(b) and (c). The overall agreement is quite good, and the calculated laser energies are close to the range of experimentally measured values shown in Table 2. In Figure 21 the experimental time-resolved laser intensity profiles for the  $H^{35}Cl$  1-0, 2-1, and 3-2 bands are plotted along with the calculated profiles for the low E/N discharge case. As seen in Figure 21(b), the calculated 1-0  $H^{35}Cl$  laser transition intensity is approximately twice that for the 2-1  $H^{35}Cl$  band. Whereas experimentally, it was found that the 2-1 transition was slightly more intense early in the laser pulse. A similar contradiction is found for the high E/N discharge case as well. Additional calculations have shown that the assumption of a large  $HCl(v=1)$  product fraction in the  $Cl+H_2(v)$  reaction is not the cause of the disagreement. The discrepancy could not be remedied by assuming only an 8 percent fractional energy distribution into  $v = 1$  from the hot reaction (see Table 3). The experimental summation shown in Figure 21 is quite sensitive to the exact peak intensities and time histories for all the lines. Hence, a slight shift (100 to 200 nsec) in a line position could strongly affect the total band intensity profile, yet only slightly alter a complete composite reconstruction as presented in Figure 8. Therefore, at present, the discrepancy presented in Figure 21 is assigned to an artifact of the data reconstruction procedure.

The calculated time history of a particular  $P(J)$  transition was typically in error by +1 or +2 in  $J$  at a given time. This was not too surprising considering the sensitivity of the gain on a particular  $J$  to

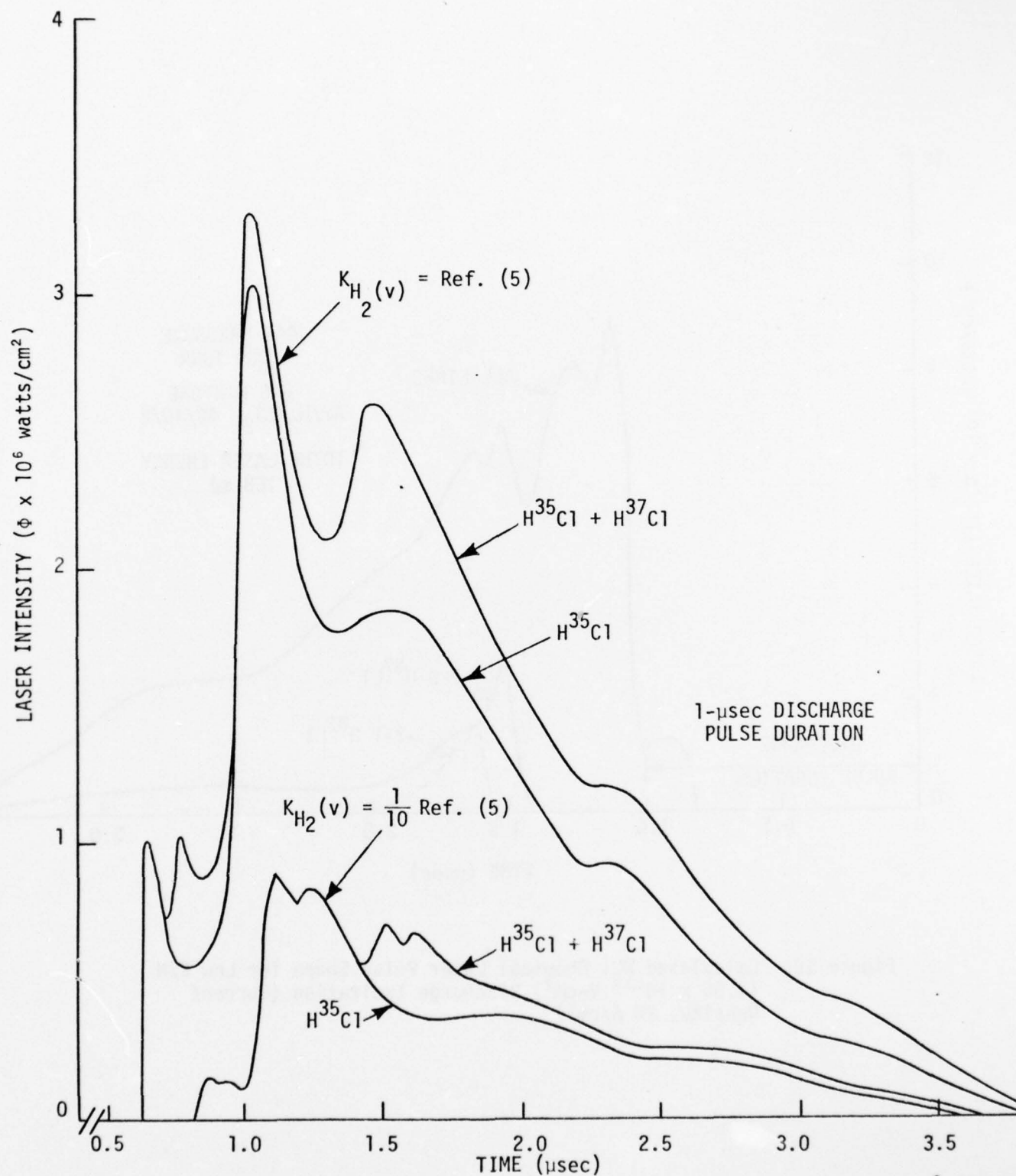


Figure 18. Calculated HCl Laser Pulse Shape for Low  $E/N$  ( $1.55 \times 10^{-16} \text{ V-cm}^2$ ) Discharge Excitation. Chlorine atom production by the discharge was 10 percent of the discharge energy input for both cases shown.

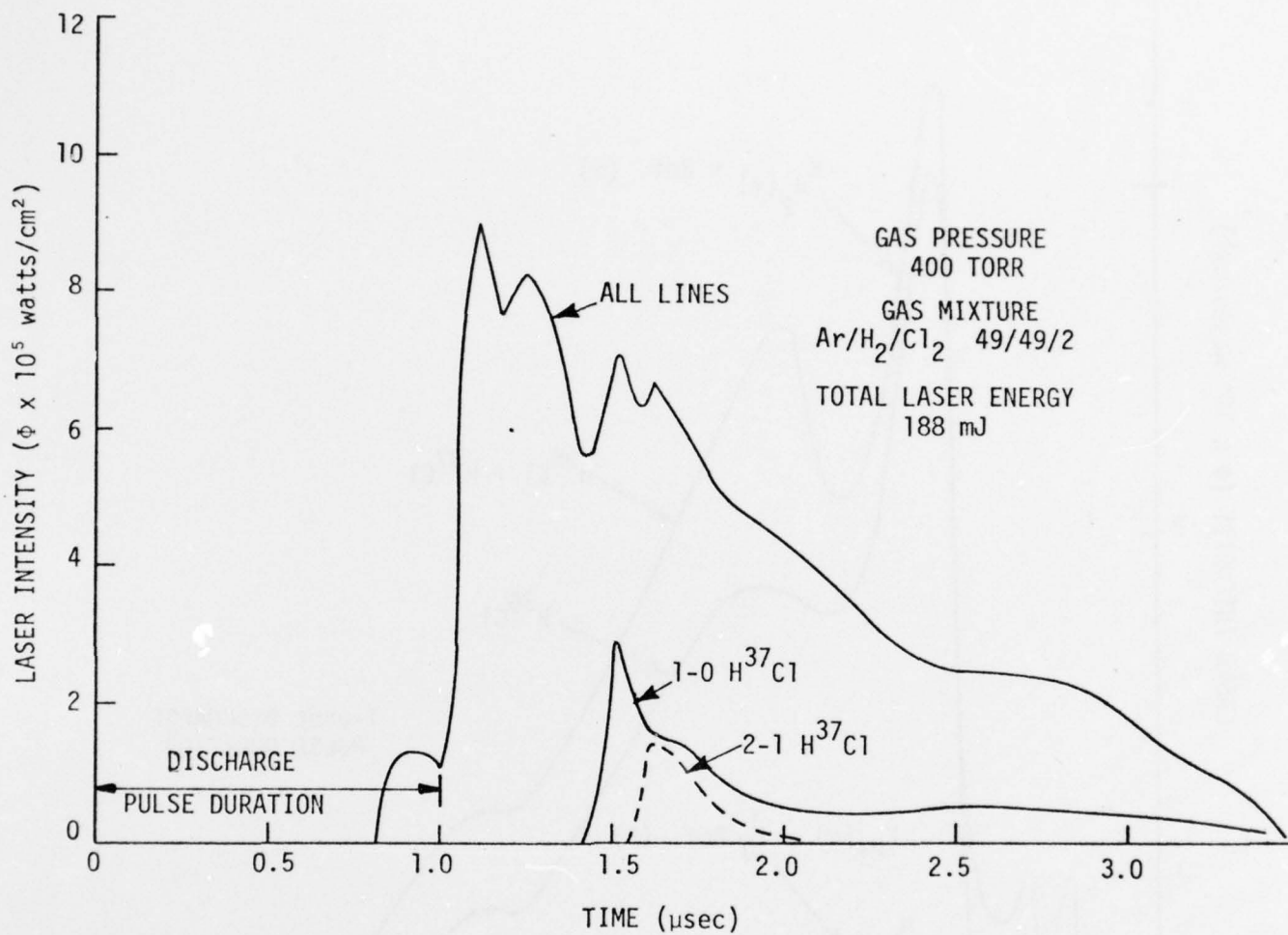


Figure 19. Calculated HCl Chemical Laser Pulse Shape for Low E/N  
 ( $1.55 \times 10^{-16}$  V-cm<sup>2</sup>) Discharge Excitation (Current  
 Density, 24 A/cm<sup>2</sup>)

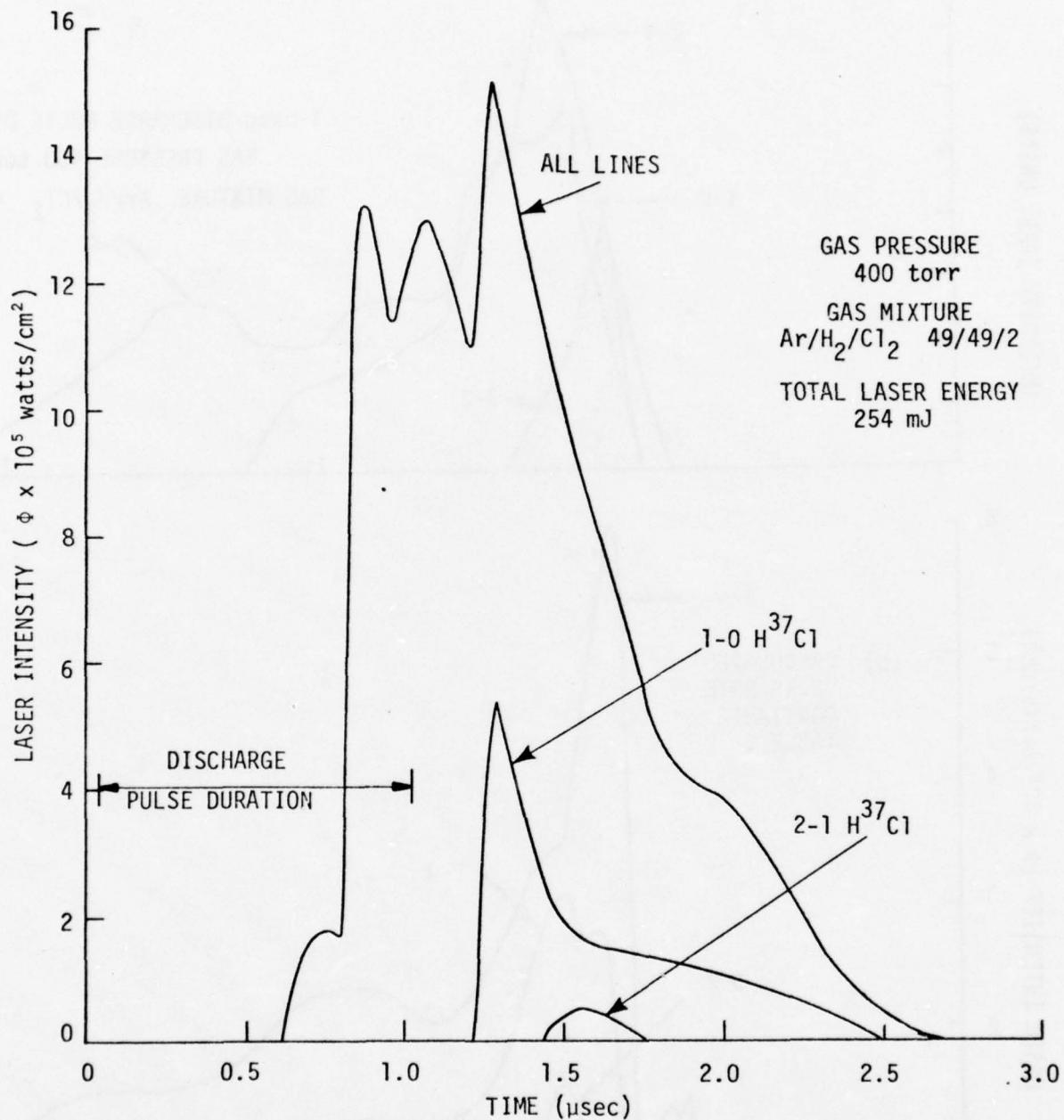


Figure 20. Calculated HCl Chemical Laser Pulse Shape for High E/N ( $2.5 \times 10^{-16}$  V-cm<sup>2</sup>) Discharge Excitation (Current Density, 24 A/cm<sup>2</sup>)



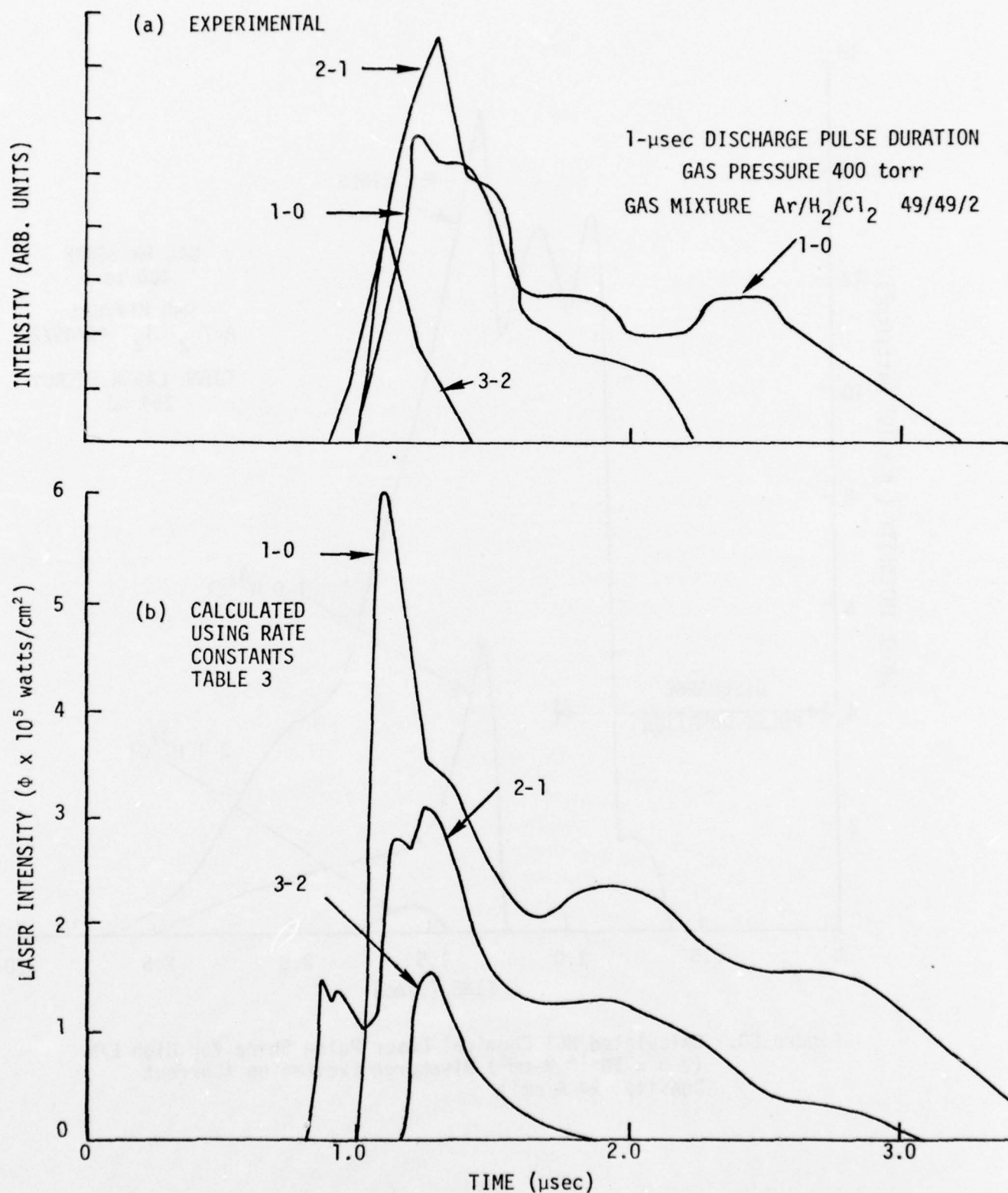


Figure 21. Comparison of Experimentally Determined Band Intensities with Calculated Profiles for the 1-0, 2-1, and 3-2 H<sup>35</sup>Cl Laser Transitions for the Low E/N ( $1.55 \times 10^{-16}$  V-cm<sup>2</sup>) Discharge Case

the inversion ratio of the two vibrational levels involved. In addition, it was found that the J time sequence could be strongly altered, depending on the choice of the collision broadening parameter. Further refinements in the model would be necessary for a more accurate tracking of the detailed P(J) time history.

The laser threshold times of the  $\text{H}^{37}\text{Cl}$  isotopes provided very sensitive criteria for establishing the H-atom production rates by the discharge. For example, in the low E/N calculations (Fig. 19), the 2-1  $\text{H}^{37}\text{Cl}$  laser transitions did not reach threshold unless the H-atom production exceeded 5 percent of the discharge energy, in addition to the H-atom production by the electron beam itself. This production rate by the discharge essentially equals the electron beam H-atom production. It could be argued that the deactivation rates chosen for  $\text{HCl}(v=2)$  were too fast and therefore higher H-atom production was necessary to overcome the losses. However, if the deactivation rates for  $v = 2$  were decreased, via lower chlorine atom production, the  $\text{H}^{35}\text{Cl}$  2-1 laser transitions did not turn off by 2.2  $\mu\text{sec}$  as found in the experimental time history (Fig. 5). The calculated  $\text{H}^{35}\text{Cl}$  2-1 laser intensity drops to 1/10 its maximum by 3.0  $\mu\text{sec}$ , which indicates that the deactivation processes for  $v = 2$  were, in fact, slightly underestimated and therefore the H-atom production rate may also have been underestimated.

Hydrogen dissociation by the low E/N discharge was calculated (see Sec. IV-A) to be 0.1 percent of the total discharge energy input, although 6 percent of the discharge energy needed to be used for hydrogen dissociation as discussed above. The high E/N Boltzmann calculations agreed very well with the 9 percent discharge energy fraction into dissociation used in the kinetics model. The large discrepancy at low E/N cannot be explained at present.

The chlorine disappearance rate helped to constrain the vibrationally enhanced rate constant. A simple kinetic analysis using the first three reactions in Table 1 yields for the  $\text{Cl}_2$  burn rate:

$$\frac{d\text{Cl}_2}{dt} = (\text{Cl}) \left[ k_{\text{H}_2(v)} (\text{H}_2(v)) + k_{\text{cold}} (\text{H}_2) \right]$$

assuming that the chlorine atom density reaches a steady state value following the discharge pulse. An estimate for the chlorine atom steady state concentration, as verified in the computer model calculations, can be obtained from Figure 22 using the initial drop in  $\text{Cl}_2$  density at approximately 1  $\mu\text{sec}$ , which leads to a value of  $4 \times 10^{-8}$  moles/c.c. The vibrational temperature of  $\text{H}_2$  calculated immediately after the discharge is approximately 2000 °K, hence the  $\text{H}_2(v)/\text{H}_2(0)$  ratio is 0.05. Therefore, the experimentally measured  $\text{Cl}_2$  disappearance rate ( $E/N = 1.6 \times 10^{-16}$  V-cm<sup>2</sup>) of  $3.4 \times 10^{-2}$  moles/c.c.-sec, implies a rate ratio ( $k_{\text{H}_2(v)}/k_{\text{H}_2(0)}$ ) of 12.5. Note that this is the rate enhancement at 350 °K, which is the calculated temperature at the end of the discharge pulse. A rate ratio of 20 at 350 °K can be calculated from the rate constants in Table 3. This is reasonably good agreement between the rate evaluation based on laser characteristics and that based on a direct  $\text{Cl}_2$  removal rate measurement.

The calculated chlorine disappearance rate using the complete kinetics code was  $4 \times 10^{-2}$  moles/c.c.-sec, which is in very good agreement with the measured values, which ranged from  $3.4 \times 10^{-2}$  to  $3.9 \times 10^{-2}$  moles/c.c.-sec. For the high  $E/N$  case, the measured disappearance rate was approximately  $9 \times 10^{-2}$  moles/c.c.-sec and the calculated rate was  $11.5 \times 10^{-2}$  moles/c.c.-sec. Ten percent of the discharge energy input for the high and low  $E/N$  cases was placed in chlorine dissociation. For the low  $E/N$  case, this corresponds to 4 percent direct chlorine dissociation by the discharge.

Wilkins,<sup>5</sup> prediction of a vibrationally excited product molecule in the reaction  $\text{Cl} + \text{H}_2(v) \rightarrow \text{HCl}(0,1) + \text{H}$  appears to be correct. If the rate of the vibrationally enhanced reaction does not include  $\text{HCl}(1)$  production, the

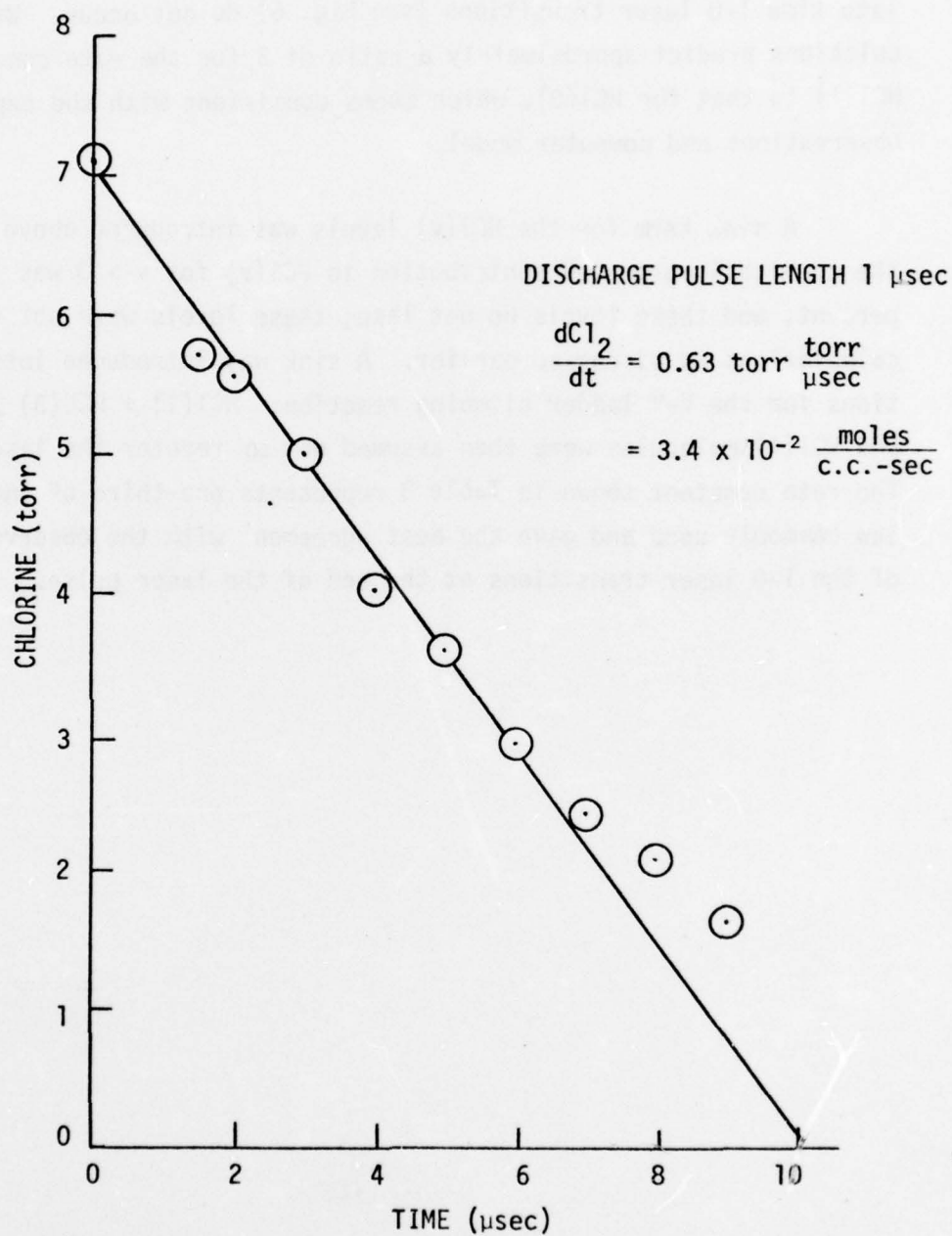


Figure 22. Rate of Chlorine Disappearance Measured in the Low  $E/N$  ( $1.55 \times 10^{-16} \text{ V-cm}^2$ ) Discharge. Gas Pressure was 400 torr and the gas mixture was  $\text{Ar}/\text{H}_2/\text{Cl}_2$  (49/49/2).



late time 1-0 laser transitions (see Fig. 6) do not occur. Wilkins' calculations predict approximately a ratio of 3 for the rate constant producing HCl(1) to that for HCl(0), which seems consistent with the experimental observations and computer model.

A sink term for the HCl(v) levels was introduced above  $v = 3$ . Since the chemically-produced contribution to HCl(v) for  $v > 3$  was less than 5 percent, and these levels do not lase; these levels were not included in the calculations as discussed earlier. A sink was introduced into the calculations for the V-V ladder climbing reaction:  $\text{HCl}(1) + \text{HCl}(3) \rightleftharpoons \text{HCl}(4) + \text{HCl}(0)$ , and HCl(4) molecules were then assumed not to reenter the laser kinetics. The rate constant shown in Table 3 represents one-third of the  $V^2$  scaling law commonly used and gave the best agreement with the observed duration of the 1-0 laser transitions at the end of the laser pulse.

## SECTION V

### CONCLUSIONS

Experimental measurements of an electrically-initiated HCl chemical laser system have been compared with a reaction kinetics-laser gain computer model. An estimate for the vibrationally-enhanced rate coefficient for the reaction  $\text{Cl} + \text{H}_2(1) \rightarrow \text{HCl}(0,1) + \text{H}$  has been derived. It is ten times smaller than a recent theoretical prediction.<sup>5</sup> However, the rate constant found is 40 times larger than the  $\text{Cl} + \text{H}_2(0)$  rate given in Table 1 ( $T=300^\circ\text{K}$ ). This finding is in qualitative agreement with an earlier experimental measurement of Stedman et al.<sup>41</sup> where a vibrational rate enhancement of "two orders of magnitude" was reported in a mass spectrometric discharge flow experiment. Sims et al.<sup>3</sup> report a theoretical rate enhancement of 23 times ( $T=300^\circ\text{K}$ ), which is only a factor of 2 smaller than the present findings. Persky and Baer<sup>4</sup> calculated a rate enhancement of 35 times, encouragingly close to the present evaluation.

Since the  $\text{Cl} + \text{H}_2(0)$  rate constant is strongly temperature dependent (see Table 3), the relative rate enhancement  $k(\text{H}_2(v))/k(\text{H}_2(0))$  decreases rapidly with increasing temperature, for example at  $400^\circ\text{K}$ , the rate ratio will decrease to 9, using Wilkins'<sup>5</sup> temperature dependence for the  $\text{Cl} + \text{H}_2(v)$  reaction. Persky and Baer<sup>4</sup> calculate a temperature-dependent rate constant ratio at  $400^\circ\text{K}$  of 13, whilst Sims et al.<sup>3</sup> report a ratio of 12.

Modelling of experiments using electron beam only initiation of the chemical laser system was dependent upon the Cl and H-atom production rates and the  $\text{H} + \text{Cl}_2$  and  $\text{Cl} + \text{H}_2$  reaction rates. The reaction rate coefficients, which gave the best agreement with experimental measurements, are shown in Table 3. Estimates for the chlorine dissociation fraction in both the electron beam and discharge-excited gas mixtures were based on measurements of the chlorine disappearance rate. Hydrogen-atom production by the electron beam was directly related to the laser energy and pulse shape and could

be fitted to the experimental observations only over a fairly narrow range (less than a factor of 2). The  $\text{H}^{37}\text{Cl}$  laser threshold time also provided a valuable benchmark for the H-atom production rate. Hydrogen-atom production in the discharge experiments were estimated a priori using published cross sections for hydrogen excitation channels in a Boltzmann calculation. Good agreement with the observed HCl laser energy and spectroscopy was obtained only by increasing the calculated dissociation fraction by a factor of 60 for the low E/N cases. For the high E/N discharge experiments, the proposed dissociation fraction was essentially the same as the value found in the Boltzmann calculation.

The value obtained in this study for the vibrationally-enhanced rate coefficient was constrained by the above considerations for the  $\text{H}+\text{Cl}_2$  and  $\text{Cl}+\text{H}_2$  rate coefficients and the H and Cl-atom production rates. It was found that the rate constant fitted to the experimental results could not be varied by more than 20 to 30 percent without serious discrepancies appearing in the laser pulse shape comparison. Wilkins,<sup>5</sup> theoretical prediction for the formation of  $\text{HCl}(1)$  in the  $\text{Cl}+\text{H}_2(v)$  reaction is consistent with experimental observation of a long "tail" on the laser pulse, consisting mainly of 1-0 laser transitions which could be duplicated in the present calculations of the laser pulse time history.

An immediate practical consequence of the smaller rate constant  $k_{\text{H}_2(v)}$  is the inherent inefficiency of the electrically-excited HCl chemical laser. Most of the energy stored in the  $\text{H}_2(v)$  is never recovered on the time scale of the laser pulse. The deactivation rate of Cl atoms predominates over other deactivation routes under the conditions of these experiments and determines the overall time constant for the laser pulse length. The maximum electrical to laser energy conversion efficiency obtained was 4.5 percent.

## REFERENCES

1. J.C. Polanyi, J. Chem. Phys. 31, 1338 (1959).
2. A.M.G. Ding, L.J. Kirsch, D.S. Perry, J.C. Polanyi, and J.L. Schrieber, Faraday Discussions of the Chemical Society 55, 252 (1973).
3. L.B. Sims, L.R. Dosser, and P.S. Wilson, Chem. Phys. Lett. 32, 150 (1975).
4. A. Persky and M. Baer, J. Chem. Phys. 60, 133 (1974).
5. R.L. Wilkins, J. Chem. Phys. 63, 2963 (1975).
6. J.G. Calvert and J.N. Pitts, Jr., Photochemistry, New York: John Wiley and Sons, p. 21, 184 (1966).
7. G.N. Whyte, Rad. Res. 18, 225 (1963).
8. M.J. Berger and S.M. Seltzer, in Studies in Penetration of Charged Particles in Matter, Nuclear Science Series Report No. 10, NAS-NRC Publ. No. 1133, National Academy of Sciences, Washington, D.C. (1964).
9. G.A. Hart and S.K. Searles, ARPA-NRL Laser Program Semiannual Technical Report to Defense Advanced Research Projects Agency, May 1975.
10. G.A. Hart and S.K. Searles, J. Appl. Phys. 47, 2033 (1976).
11. S.K. Searles, private communication.
12. A.A. Christodoulides, R. Schumacher and R.N. Schindler, J. Phys. Chem. 79, 1904 (1975).
13. G.D. Sides, T.O. Tiernan and R.J. Hanrahan, J. Chem. Phys. 65, 1966 (1976).
14. E. Schultes, A.A. Christodoulides, and R.N. Schindler, Chem. Phys. 8, 354 (1975).
15. C.J. Howard, F.C. Fehsenfeld, and M. McFarland, J. Chem. Phys. 60, 5086 (1974).
16. A.G. Englhardt and A.V. Phelps, Phys. Rev. 133, A375 (1964).
17. D.K. Gibson, Australian J. Phys. 23, 683 (1970).



18. F. Linder and H. Schmidt, *Z. Naturforsch* 269, 1603 (1971).
19. S. Chung, C.C. Lin and E.T.P. Lee, "Dissociation of the Hydrogen Molecule by Electron Impact," (submitted *Phys. Rev.*).
20. J.S. Whittier, M.L. Lundquist, A. Ching, G.E. Thornton, and R. Hofland, Jr., *J. Appl. Phys.* 47, 3542 (1976).
21. N. Cohen and J.F. Bott, "A Review of Rate Coefficients in the H<sub>2</sub>-Cl<sub>2</sub> Chemical Laser System," Aerospace Laboratory Report No. SAMSO-TR-75-82, El Segundo, California, March 19, 1975.
22. K.G. Anlauf, D.S. Horne, R.G. Macdonald, J.C. Polanyi, and K.B. Woodall, *J. Chem. Phys.*, 57, 1561 (1972).
23. S.R. Leone and C.B. Moore, *Chem. Phys. Lett.* 19, 340 (1973).
24. P.F. Zittel and C.B. Moore, *J. Chem. Phys.* 59, 6636 (1973).
25. H.-L. Chen and C.B. Moore, *J. Chem. Phys.* 54, 4072 (1971).
26. J.F. Bott and N. Cohen, *J. Chem. Phys.* 63, 1518 (1975).
27. R.V. Steele, Jr. and C.B. Moore, *J. Chem. Phys.* 60, 2794 (1974).
28. J.F. Bott and R.F. Heidner, *J. Chem. Phys.* 64, 1544 (1976).
29. D. Arnoldi and J. Wolfrum, *Chem. Phys. Lett.* 24, 234 (1974).
30. R.G. Macdonald and C.B. Moore, private communication.
31. R.D.H. Brown, G.P. Glass and I.W.M. Smith, *J. Chem. Soc., Faraday Trans.* 71, 1963 (1975).
32. J.V.V. Kasper, in Proceedings of Army Symposium on High Energy Lasers: Current Problems in High Energy Transfer Lasers, Special Report RH-7T-1, U.S. Army Missile Command, Redstone Arsenal, Alabama, August 1976.
33. G. Herzberg, Spectra of Diatomic Molecules, New York: Van Nostrand (1950).
34. J.M. Herbelin and G. Emanuel, *J. Chem. Phys.* 60, 689 (1974).
35. H. Babrov, G. Ameer, and W. Benesch, *J. Chem. Phys.* 33, 145 (1960).
36. A. Levy, E. Piollet-Mariel and C. Boulet, *J. Quant. Spectrosc. Radiat. Transfer* 13, 673 (1973).

37. W.S. Benedict, R.C. Herman, C.E. Moore, and S. Silverman, Can. J. Phys. 34, 850 (1956).
38. M.A.A. Clyne and R.F. Walker, J. Chem. Soc., Faraday Trans. 69, 1547 (1973).
39. J. Wilson, H.-L. Chen, W. Fyfe, R.L. Taylor, R. Little, and R. Lowell, J. Appl. Phys. 44, 5447 (1973).
40. R. Hofland, M.L. Lundquist, A. Ching, and J.S. Whittier, J. Appl. Phys. 45, 2207 (1974).
41. D.H. Rank, D.P. Eastman, B.S. Rao, and T.A. Wiggins, J. Mol. Spectrosc. 10, 34 (1963).

PART B

THRESHOLD POWER DENSITY MEASUREMENTS FOR  
ELECTRON BEAM SUSTAINED DISCHARGE  
EXCITATION OF XeF AND KrF

PART B  
CONTENTS

SECTION		PAGE
I	INTRODUCTION	1
II	DESCRIPTION OF EXPERIMENT	2
III	EXPERIMENTAL RESULTS	7
	A. XeF Laser Threshold Measurements	7
	B. KrF Laser Threshold Measurements	7
IV	DISCUSSION	12
	REFERENCES	18



## PART B

### FIGURES

FIGURE		PAGE
1.	Experimental Layout for KrF and XeF Threshold Pumping Measurements	3
2.	Temporal Variation of e-Beam Voltage and Current, Discharge Voltage and Current, and Photodiode Signal for an Ar + 0.5% Xe + 0.1% NF <sub>3</sub> Gas Mixture at 1 atm	6
3a.	Threshold Electric Discharge Power Density for XeF Laser Emission as a Function of NF <sub>3</sub> Concentration for Fixed Xe/NF <sub>3</sub>	8
3b.	Threshold Electric Discharge Power Density for XeF Lasing as a Function of Xe Concentration for Fixed NF <sub>3</sub>	9
4.	Threshold Electric Discharge Power Density Measurements for KrF Laser Emission as a Function of F <sub>2</sub> Concentration	10
5.	Pump Power Density as a Function of Delay Time for XeF Lasing	13

PART B

TABLE

TABLE

PAGE

1. XeF Laser Output Energy for Two Pump Power Densities

16

## SECTION I

### INTRODUCTION

Self-sustained and UV preionized discharge techniques for excitation of the rare gas halide lasers, e.g., KrF, XeF, and ArF, have proved very useful for small laser systems but appear to be limited to pulse energies less than 1 J. At present, the only viable scheme for higher pulse energies and high average power appears to be the electron-beam sustained discharge. It has been shown that the discharge physics in mixtures of the rare gases and halogen containing molecules is dominated by electron impact excitation and ionization of the rare gas metastables, leading to an effective upper bound on the applied E/N of the discharge to avoid instabilities.<sup>1</sup> In order to achieve long-term stable discharges, it appears necessary to operate at modest pump power density and a sufficiently large gain length in order to saturate the medium. This is in contrast with the early experiments on electron-beam ionized discharge excitation of KrF which involved input power densities of the order of 1 MW/cm<sup>3</sup> and excitation pulse length limited to approximately 100 nsec by discharge instabilities. The present measurements were undertaken in order to investigate the minimum threshold power density required to achieve stimulated emission in both KrF and XeF for long pulse excitation (~ 1  $\mu$ sec) by the electron-beam sustained discharge technique.

## SECTION II

### DESCRIPTION OF EXPERIMENT

A schematic of the experimental apparatus is shown in Figure 1. The cold cathode electron gun was described in the previous section dealing with the HCl laser work. It was operated with a 3 cm cathode to anode spacing at a Marx voltage of 160 kV. This resulted in a 1- $\mu$ sec, 4-amp/cm<sup>2</sup> ionization pulse for the discharge. The current density through the aluminized Kapton foil was estimated by simultaneously measuring the energy deposition with a calorimeter and the temporal history with a current transformer. The e-beam uniformity was verified by firing the gun into a piece of Ozalid paper placed adjacent to the discharge cathode screen. It was found necessary to sandpaper the graphite cathode on the electron gun each time a foil ruptured in order to ensure a uniform current distribution through the foil.

The discharge chamber was constructed of high density polyethylene, which provides a passive surface for the highly reactive fluorine. The nominal discharge volume is 625 cm<sup>3</sup> and is formed by a 50-cm x 5-cm aluminum anode spaced 2.5 cm from a screen cathode adjacent to the electron beam foil window. The discharge cell was fitted with fused silica or calcium fluoride windows at Brewster's angle, leaving an inactive 12 cm region at each end of the discharge. The fused silica windows were attacked by the fluorine containing gas mixtures and had to be changed frequently, while the calcium fluoride windows showed little evidence of damage. A stable optical cavity was obtained by the use of 2-m radius-of-curvature mirrors spaced 1.3 m apart or a 2-m radius-of-curvature mirror opposite a flat mirror at the same separation. The maximum reflectance mirrors for the KrF experiments (coated for 2500 Å) had a loss of 3 percent while the corresponding mirrors for XeF (coated for 3500 Å) had less than 1 percent loss. Output coupling mirrors with transmissions of 12 and 30 percent were also available for the KrF and XeF experiments, respectively.



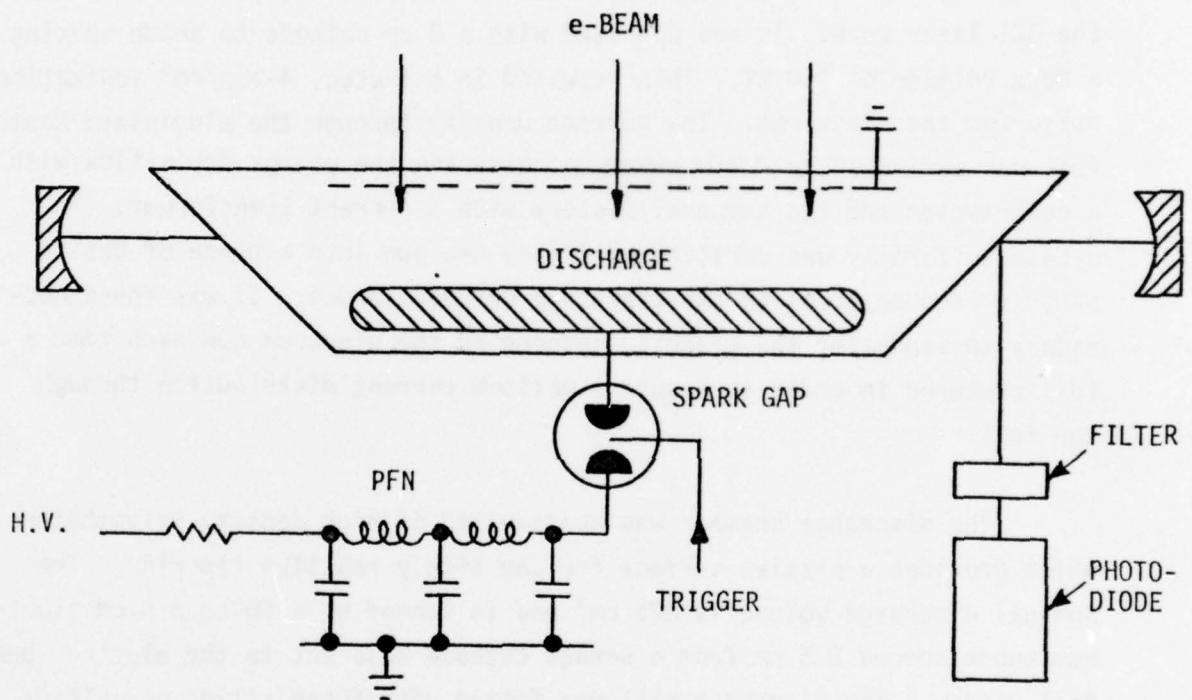


Figure 1. Experimental Layout for KrF and XeF Threshold Pumping Measurements

All of the present experiments were performed at a total gas pressure of 1 atm in order to minimize the number of foil failures. The KrF experiments were performed in mixtures of Kr and  $F_2$  diluted in Ar while most of the XeF experiments were performed in mixtures of Xe and  $NF_3$  diluted in Ar. Some preliminary experiments using  $NF_3$  and  $F_2$  as the F donor for the XeF experiments indicated higher efficiency with  $NF_3$ . The Ar diluent was used to provide a high stopping power for the electron beam ionization.

The gases were prepared in a high-purity stainless steel manifold and then allowed to sit until diffusive mixing had taken place. The entire manifold was thoroughly passivated by filling it with gradually increasing fluorine concentrations ending up with an exposure of several hours at a fluorine pressure of 250 torr. Disposal of the fluorine was accomplished by pumping it slowly through a charcoal trap where it rapidly reacts with the charcoal to form volatile fluorinated hydrocarbons. The discharge chamber was passivated by following the same procedure described for the gas handling manifold. The effectiveness of this passivation was verified by placing an Ar + 1%  $F_2$  gas mixture in the discharge chamber and monitoring the absorption of the Hg 2537 Å resonance line by  $F_2$ . Before the discharge chamber was passivated, the  $F_2$  disappeared within two or three minutes after being added. However, after the discharge chamber was cleaned and passivated, there was no detectable loss of  $F_2$  for times as long as 20 minutes after filling, even when several e-beam sustained discharge pulses were fired into the gas. The UV absorption scheme was also used to verify the composition of the premixed gases and indicated that the gas mixing manifold was well passivated.

The discharge energy for these experiments was supplied with two different pulse forming networks--one with a pulse duration of approximately 100 nsec and the other with a pulse duration of about 1  $\mu$ sec. The initial work was carried out with the 100 nsec network because it was possible to construct the pulser from parts already on hand while we waited for delivery of the capacitors for the 1  $\mu$ sec line. The 100 nsec network was constructed

from twenty 2.4 nF door-knob capacitors with a voltage rating of 40 kV. The capacitors were connected between two parallel plates of 0.030 in. thick galvanized steel and were arranged in five rows such that the characteristic impedance  $Z = \sqrt{L/C} \sim 1 \Omega$ . The 1  $\mu$ sec pulser consisted of five 0.2  $\mu$ f capacitors equally spaced along a five-turn solenoid with a coaxial return path, which resulted in a characteristic impedance of approximately 1  $\Omega$ . For the threshold measurements, two of the capacitors were disconnected from one end of the line, which shortened the pulse duration to about 600 nsec. The discharge current was monitored by measuring the voltage drop across the low inductance stainless steel resistor in series with the return side of the line. The discharge voltage was measured with a resistive divider connected to the anode. Comparison of this divider with a Tektronix (P6015) high-voltage probe indicates that it had a rise time of 50 nsec or less, which is adequate for the pulse durations of this work. The pulse-forming network was discharged into the gas via a spark gap triggered at a controlled delay time (usually about 200 nsec) following the initiation of the e-beam pulse.

Voltage and current monitors were used on the electron beam and the electric discharge while a photodiode (ITT F4000 S-5) was used as the primary diagnostic to monitor the cavity flux scattered from one of the Brewster angle windows. Oscillograms displaying the typical temporal variation of these parameters are shown in Figure 2. The threshold pump power density was determined by reducing the discharge electric field to the point where stimulated emission was barely discernible within the discharge pulse width. One drawback in these experiments was the necessity to vary the applied E/N in order to vary the input power density at the fixed current density of the electron gun. The applied electric fields were typically in the range of 1.5 to 3 kV/cm-atm, with the higher electric fields being achieved at the higher concentrations of  $F_2$  and  $NF_3$ .

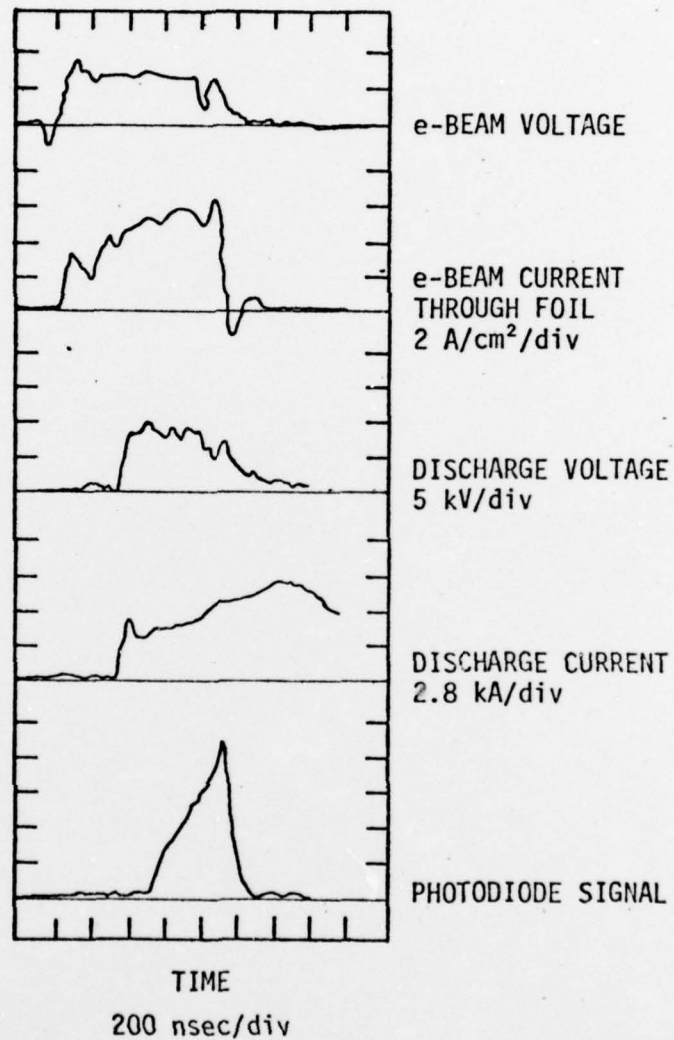


Figure 2. Temporal Variation of e-Beam Voltage and Current, Discharge Voltage and Current, and Photodiode Signal for An Ar + 0.5% Xe + 0.1% NF<sub>3</sub> Gas Mixture at 1 atm



### SECTION III

#### EXPERIMENTAL RESULTS

##### A. XeF Laser Threshold Measurements

Threshold discharge power density measurements for lasing in XeF are shown in Figures 3a and 3b for varying  $\text{NF}_3$  concentration at fixed  $\text{Xe}/\text{NF}_3$  ratio and for varying  $\text{Xe}/\text{NF}_3$  ratio at fixed  $\text{NF}_3$  concentration. Measurements were made with both the maximum reflectance cavity and with 30 percent output coupling. Threshold lasing by e-beam excitation alone was achieved in the maximum reflectance cavity for the 0.05% and 0.1%  $\text{NF}_3$  concentrations, the e-beam input power density being approximately  $30 \text{ kW/cm}^2$ . The discharge threshold measurements for these cases give an upper bound and correspond to the power density necessary to significantly increase the output and to obtain the threshold delay time of several hundred nanoseconds characteristic of all the measurements. The lack of lasing with e-beam only excitation for  $\text{NF}_3$  concentrations greater than 0.1 percent suggests collisional quenching of  $\text{XeF}^*$  or some other competition involving  $\text{NF}_3$  that reduces the gain. However, in no case was threshold lasing achieved by the e-beam alone when a 30 percent output coupler was used. These measurements, therefore, represent true threshold conditions for the given electron-beam current density and excitation pulse length of the order of 1- $\mu\text{sec}$ . The discharge threshold power densities are typically one-half to two-thirds the e-beam input power density.

##### B. KrF Laser Threshold Measurements

Threshold data for experiments in KrF are shown in Figure 4 for  $\text{F}_2$  concentrations ranging from 0.1 to 0.8 mole percent, with a fixed Kr concentration of 6 percent. These mixtures span typical gas mixtures used in previous e-beam sustained discharge laser experiments. Measurements were

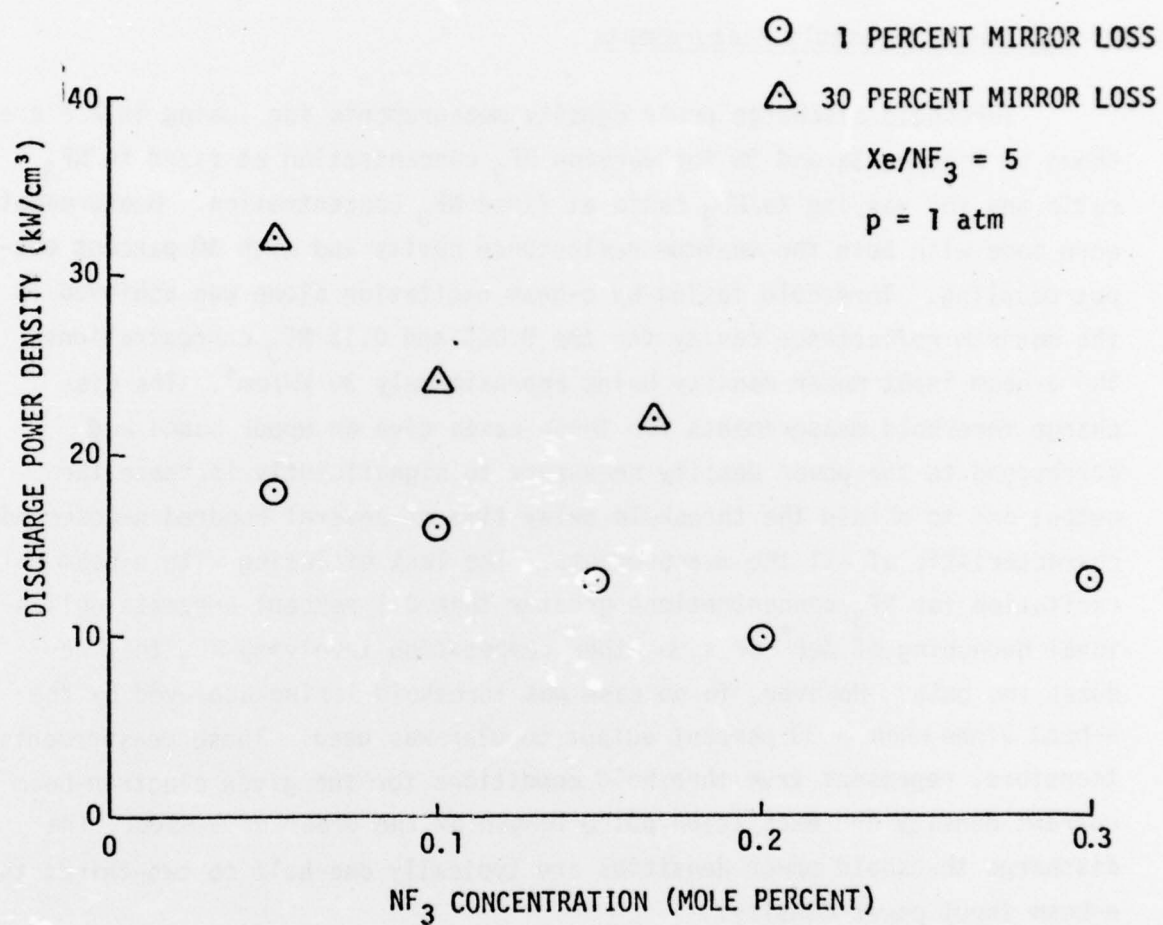


Figure 3a. Threshold Electric Discharge Power Density for XeF Laser Emission as a Function of NF<sub>3</sub> Concentration for Fixed Xe/NF<sub>3</sub>

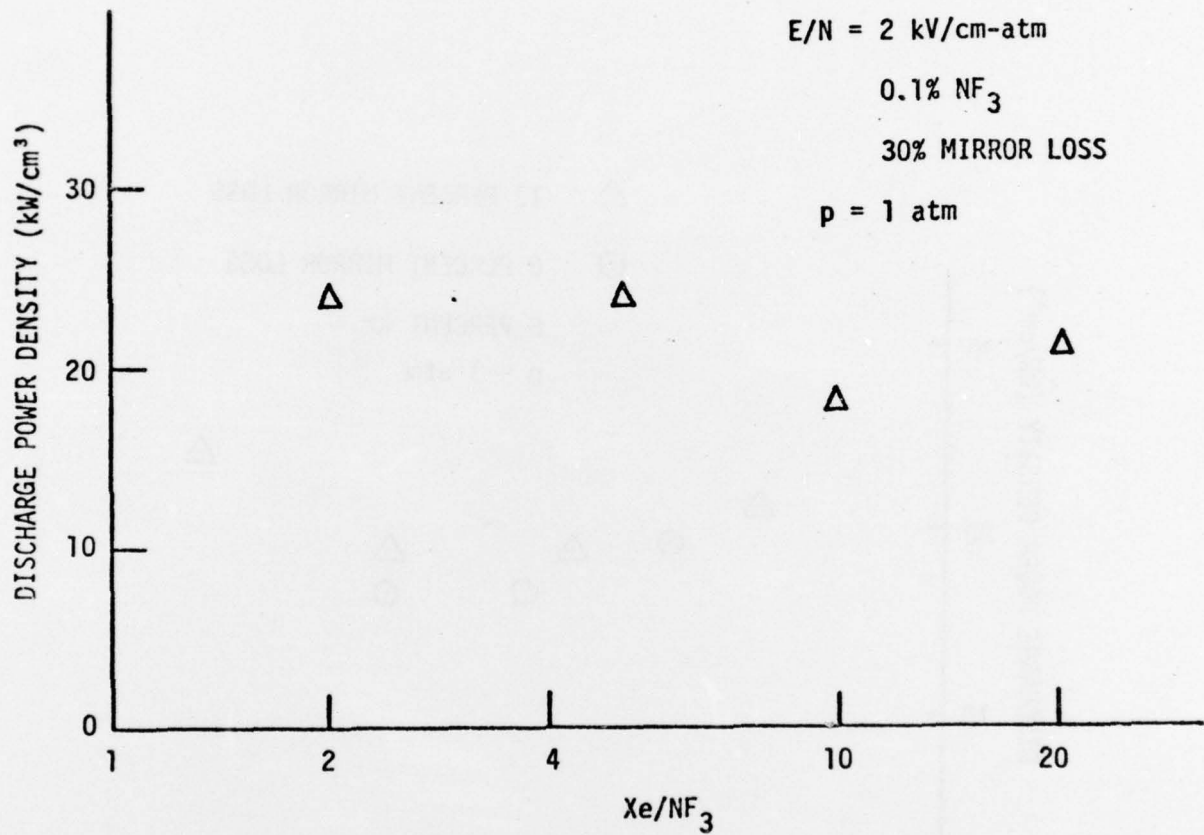


Figure 3b. Threshold Electric Discharge Power Density for XeF Lasing as a Function of Xe Concentration for Fixed  $NF_3$

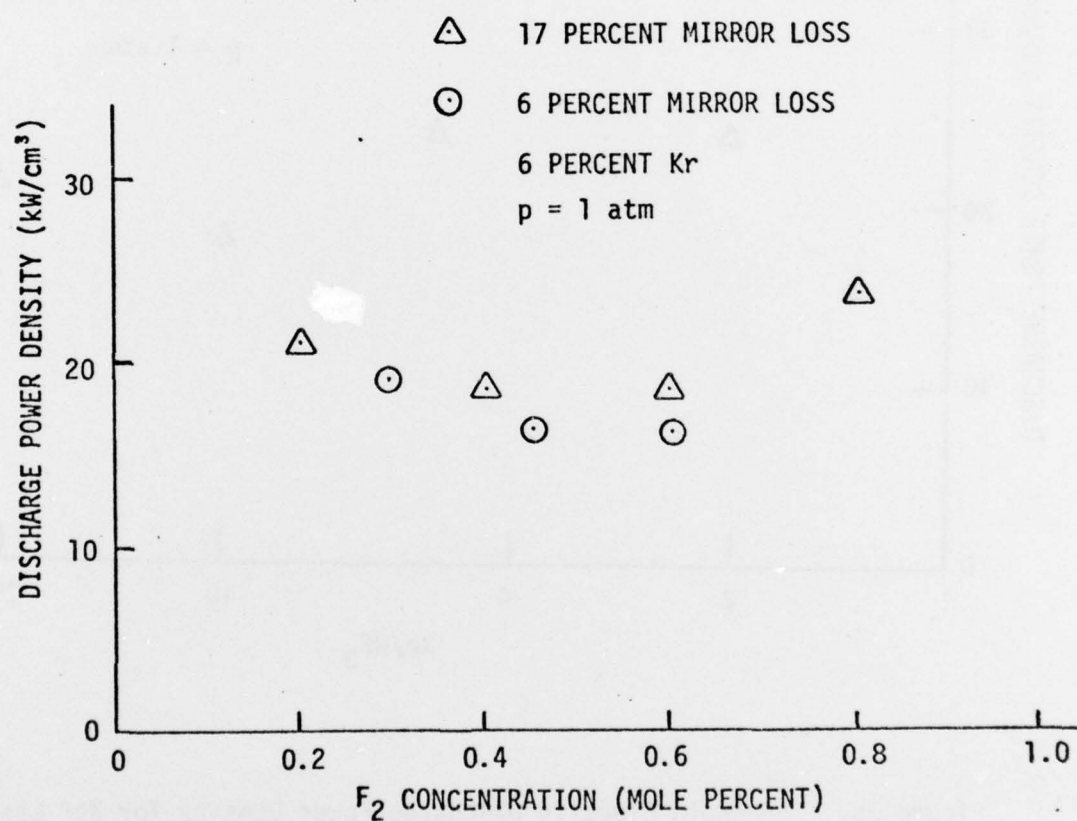


Figure 4. Threshold Electric Discharge Power Density Measurements for KrF Laser Emission as a Function of F<sub>2</sub> Concentration. The Kr concentration was fixed at 6 percent.



made with both the maximum reflectance cavity and with a 12 percent output coupler. Threshold lasing was readily achieved by the e-beam alone for  $F_2$  concentrations of 0.2 percent or less in both cavities and, therefore, only an upper bound can be set to the threshold discharge power density. Discharge pumping was always necessary to achieve threshold conditions for  $F_2$  concentrations of 0.3 percent or more. In contrast to the situation noted previously for XeF, the lack of lasing at higher  $F_2$  concentrations may be attributed to absorption at the laser wavelength due to  $F_2$ . It should be noted that the threshold measurements for the high  $F_2$  concentrations also represent an upper bound due to absorption of the stimulated emission by  $F_2$  in the inactive end regions of the discharge. This single pass loss by absorption is approximately 10 percent per mole percent of  $F_2$ .

## SECTION IV

### DISCUSSION

The measured laser threshold power densities in KrF and XeF are considerably smaller than those reported for a shorter active discharge length<sup>2,3</sup> and are also smaller than those measured in the present device with a short pulse (approximately 100 nsec) discharge supply. Pump power densities for several different XeF experiments are plotted in Figure 5 as a function of  $\ell t/\tau$ , where  $t$  is the time to reach threshold measured from the start of the discharge pulse,  $\ell$  is the active gain length, and  $\tau$  is the cavity round trip time. The pump power densities are the sum of the discharge and e-beam contributions. The e-beam deposition was estimated from the tables of Berger and Seltzer<sup>4</sup> and then multiplied by a factor of 2.5 to account for multiple scattering effects.<sup>5</sup>

These experiments can be interpreted as follows. At 1 atm pressure the primary loss mechanism in the absence of stimulated emission is radiative decay for lifetimes of the order of 10 nsec. The dominant collision partner for deactivation of the lasing species is probably  $F_2$  or  $NF_3$ , and collision cross sections in excess of gas kinetic would be required for collisional deactivation to compete with radiative decay. Thus, the time to reach threshold lasing conditions from the onset of the discharge excitation is determined by the number of round trips necessary to build up the cavity flux so that it exceeds the radiative loss and can thus begin to saturate the transition. Provided that the mirror losses are small compared to the round trip gain, the delay time can then be estimated in terms of the small signal gain from the expression

$$\frac{\pi}{\theta^2} = \left\{ R \exp[2(g_0 - \alpha)\ell] \right\}^{t/\tau}$$

where  $\theta$  is the half-angle defining the internal modes that are stable within the cavity,  $R$  is the net round-trip reflectivity in the cavity, including all losses, and  $g_0$  and  $\alpha$  are the small signal gain and absorption, respectively.

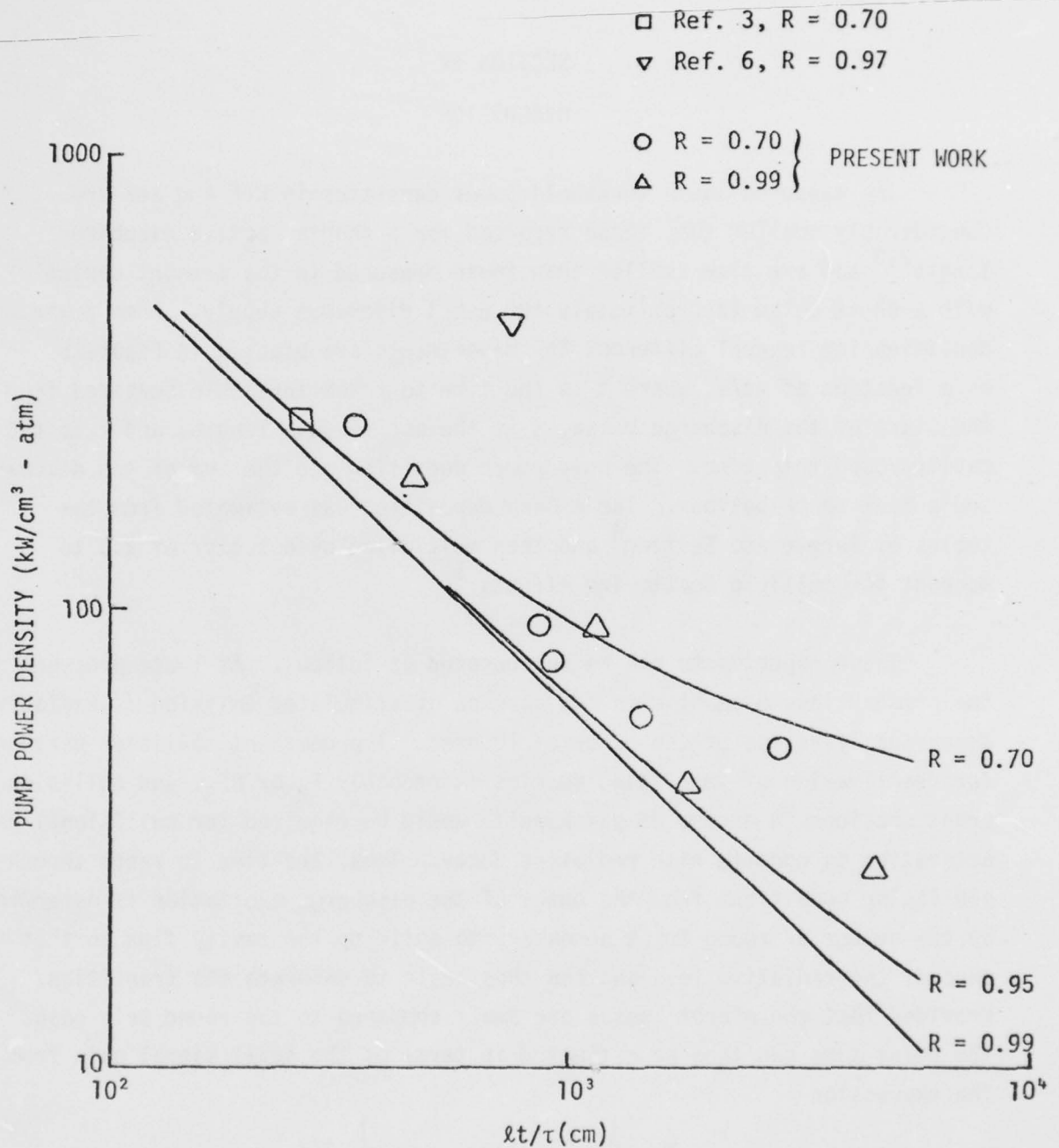


Figure 5. Pump Power Density as a Function of Delay Time for XeF Lasing. The continuous curves are values of the small signal gain as a function of  $lt/\tau$  calculated from the equation presented in the text for  $l = 50$  cm,  $\tau = 8.7$  nsec, and  $\theta = 5$  mrad. The scales for the small signal gain and pump power density have been arbitrarily adjusted with respect to each other to illustrate the functional dependence.

Since the small signal gain is directly proportional to the input power density, it is evident that threshold is defined by the constant product of the input power density and the delay time  $t$ . Under these circumstances, threshold conditions are effectively determined by the input energy density.

To test this analysis, we have plotted as continuous curves in Figure 5, values of the small signal gain  $g_0$  as a function of  $lt/\tau$  calculated from the above equation for three reflectivities and a cavity half angle of 5 milliradians. The scales for the small signal gain and the pump power density were arbitrarily adjusted with respect to each other to illustrate the functional dependence. With the exception of the electron-beam pumped experiment of Brau and Ewing<sup>6</sup>, the data follow the predicted trend. The implication of this analysis is that the threshold pump power densities measured in these experiments can be applied to other experimental systems using the above relationships. It should be noted that for a well designed cavity, increasing the path length does not change  $l/\tau$ . Thus, the threshold pump power is independent of length and is determined by the maximum permissible delay time consistent with discharge stability.

Since we have measured the delay time,  $t$ , it is possible to estimate a small signal gain in the present experiments using the above equation. This leads to small signal gains of the order of 1 percent/cm and thus satisfies the requirement that the round-trip gain be much larger than the mirror loss.

It is also possible to roughly estimate the gain from the input pump power density. The electric discharge energy produces metastable  $\text{Ar}^*$  with an efficiency of approximately 25 percent (Ref. 3). About 75 percent of the  $\text{Ar}^*$  reacts with Xe to form  $\text{Xe}^*$ , which subsequently reacts with  $\text{NF}_3$  to form  $\text{XeF}^*$ . If radiative loss of  $\text{XeF}^*$  is dominant, then at steady state the small signal gain is approximately



$$g_0 = \sigma[\text{XeF}^*] \cong \sigma \left[ \frac{\eta P \tau_{\text{XeF}}}{E_{\text{Ar}^*}} \right] \cong 1\%/\text{cm}$$

where  $P = 15 \text{ kW/cm}^3$  is the discharge power density,  $\eta = (0.25) \times (0.75)$  is the product of the efficiency of discharge production of  $\text{Ar}^*$  with the branching ratio for conversion of  $\text{Ar}^*$  to  $\text{Xe}^*$ ,  $E_{\text{Ar}^*} = 11 \text{ eV/molecule}$  is the  $\text{Ar}^*$  excitation energy, and  $\sigma \tau_{\text{XeF}^*} = 7.5 \times 10^{-24} \text{ cm}^2\text{-sec}$  is the product of the  $\text{XeF}^*$  stimulated emission cross section and radiative lifetime (this product is independent of  $\tau_{\text{XeF}}$  since  $\sigma \sim 1/\tau_{\text{XeF}^*}$ ).

In the case of e-beam excitation, the energy is deposited by ionization of the Ar diluent. For an average energy loss of 26 eV per ionization, the estimated e-beam input power density of  $30 \text{ kW/cm}^3$  corresponds to an  $\text{Ar}^+$  production rate of  $7 \times 10^{21} \text{ Ar}^+ \text{ cm}^{-3}\text{-sec}^{-1}$ . The branching ratio to form  $\text{XeF}^*$  is not yet known; however, if it is assumed to be unity, then at steady state, the small signal gain would be approximately

$$g_0 = \sigma[\text{XeF}^*] \sim \sigma[R \tau_{\text{XeF}^*}] = (7.5 \times 10^{-24} \text{ cm}^2\text{-sec})(7 \times 10^{21} \text{ cm}^{-3} \text{ sec}^{-1}) \sim 5\% \text{ cm}^{-1}$$

This is much higher than the small signal gain estimated from the delay time analysis, which implies that the branching ratio for  $\text{Ar}^+$  conversion to  $\text{XeF}^*$  is significantly less than unity. There is presently not enough information about the steps in the kinetic chain responsible for  $\text{XeF}^*$  formation to allow an assessment of what process is responsible for this inefficiency.

In addition to the above threshold power density measurements, some experiments were made with 30 percent output coupling to measure the pulse energy and efficiency in  $\text{XeF}$ . The experimental conditions for two measurements made with both the 100 nsec and 500 nsec pulse-forming network power supplies are presented in Table 1. Maximum pulse energies of approximately 35 mJ were extracted from an active optical volume of 0.19 l corresponding to an energy density of 0.18 J/l-atm. The electrical efficiency defined by the

Table 1

XeF Laser Output Energy for Two Pump Power Densities

Gas Mixture	Ar+1.2% Xe+0.25% NF <sub>3</sub>	Ar+1% Xe+0.1% NF <sub>3</sub>
Power Supply	100 NSEC PFN	500 NSEC PFN
Discharge Voltage (kV/cm-atm)	3	2
Discharge Power (kW/cm <sup>3</sup> -atm)	230	60
E-Beam Power (kW/cm <sup>3</sup> -atm)	30	30
Discharge Energy (J/l-atm)	28	20
E-Beam Energy (J/l-atm)	5	10
Laser Energy (mJ)	25	35
(J/l-atm)	0.13	0.18
Electrical Efficiency	0.4%	0.6%

ratio of lasing energy extracted divided by total energy deposited in the same volume was approximately 0.5 percent. These experiments were made with an applied electric field of approximately 2 kV per cm-atm and with the discharge input power density a factor of 2 larger than the e-beam power density. The lasing pulse lengths of these experiments were approximately 100 to 200 nsec, the discharge becoming unstable after approximately 300 nsec. It should be observed that no special precautions were taken to optimize the discharge geometry and thereby minimize the field concentration, as might be achieved by careful shaping of the discharge electrodes.

Based on the present results for the threshold pump power density, it is evident that efficient laser operation in KrF and XeF could be achieved in a 1-m long e-beam sustained discharge with input power densities in the range of 50 to 100 kW/cm<sup>3</sup> over a 1- $\mu$ sec time scale. Stable discharges have been operated in KrF and XeF at these power densities which are an order of magnitude smaller than the power densities used in short pulse (100 nsec or less) e-beam sustained discharges.

## REFERENCES

1. J. D. Daugherty, J. A. Mangano, and J. H. Jacob, Appl. Phys. Lett. 28, 581 (1976).
2. J. A. Mangano and J. H. Jacob, Appl. Phys. Lett. 27, 495 (1975).
3. J. A. Mangano, J. H. Jacob, and J. B. Dodge, Appl. Phys. Lett. 29, 427 (1976).
4. M. J. Berger and S. M. Seltzer, Studies in Penetration of Charged Particles in Matter, Nuclear Science Series Report No. 10, NAS-NRC Publ. 1133, National Academy of Sciences, Washington, D. C. 1964.
5. G. A. Hart and S. K. Searles, J. Appl. Phys. 47, 2033 (1976).
6. C. A. Brau and J. J. Ewing, Appl. Phys. Lett. 27, 437 (1975).